Thermal properties of candidate coolant salts

Cathleen E. Ridder

Thesis submitted to the Faculty of the

Virginia Polytechnic Institute and State University

in partial fulfillment of the requirements for the degree of

Master of Science

In

Nuclear Engineering

Jinsuo Zhang, Chair

Amanda Leong

Alireza Haghighat

July 2, 2024

Blacksburg, Virginia

Keywords: Molten Salt Reactors, Thermal Properties, Vapor Pressure, Heat Capacity, Density, Melting Point,

Thermal Properties of Candidate Coolant Salts

Cathleen E. Ridder

(ABSTRACT)

With the increasing research on advanced reactors, molten salt reactors have been recognized for their potential. As with any advanced reactor concept, each component and material must be thoroughly investigated before any reactors of that type are created. One of the most pressing issues in MSR research is that of the salts themselves. Though there are a multitude of salts to choose from when designing such a reactor, many of these salts lack the extensive research required to fully understand them. Across the decades there have been many studies that have investigated select molten salts, but there are a few problems with many of those studies. Those problems are the following: prior papers use obsolete and less reliable methods for their measurements, the papers don't investigate the salts across a wide enough range of temperatures nor at varying compositions, and finally many of the salts that are seen as candidates today were not given as much attention when molten salt reactors were first conceptualized which has resulted in a lack of research on them. Indeed, the research into these salts is lacking in many ways. This study seeks to investigate a collection of promising coolant salts in depth with acknowledgment to those past studies. LiF-NaF-KF (46.5-11.5-42.0 mol%) will be used as a calibration standard and for the purpose of verifying our methodology. Specifically, FLiNaK was used in the development of volume-height curves as calibration for density measurements. NaOH-KOH of four different compositions (0.5-0.5mol%, 0.55-0.45mol%, 0.6-0.4mol%, and 0.65-0.35 mol%) will be evaluated for their densities and heat capacities. And finally, BeF_2-NaF(43-57mol%) will be evaluated within the question of if the properties are desirable enough that the dangers posed by beryllium are an acceptable risk. BeF_2-NaF will have melting point, heat capacity, density, and vapor pressure measurements performed. Additionally, extensive impurity analysis and removal (via an HF gas system) was done to our BeF_2-NaF samples. The melting point and heat capacity were evaluated using dynamic scanning calorimetry (DSC), the vapor pressure was evaluated using thermogravimetric analysis (TGA), and the density was measured using a system similar to the Arrhenius method that measures height.

Thermal Properties of Candidate Coolant Salts

Cathleen E. Ridder

(General Audience Abstract)

Decades have passed since the discussion of nuclear energy began. Although great progress has been made in the field, the nuclear reactors in use today consist mainly of boiling water reactors (BWRs) or pressurized water reactors (PWRs). As reliable as these reactors have become, one can no longer ignore the fact that there is a multitude of other options for how a reactor can be built and operated. Options that provide greater safety and more energy output. Many reactor concepts of the past were discounted for the extensive research that would be required to make use of them. However, as time has passed and technology has improved, that research has become more and more possible. Many advanced reactors are the result of that attention to the reactor concepts and materials of the past that couldn't be given the attention that they deserve until now. Molten salt reactors (MSRs) are one of those promising concepts. However, before they can be built every part of the reactor, from the structure to the materials, must be entirely understood. One of the most pressing issues in MSR research is the properties of the salts in consideration for use. Though there are a multitude of salts to choose from when designing such a reactor, many of these salts lack the extensive research required to fully understand them. Across the decades there have been many studies that have investigated select molten salts, but there are a few problems with many of those studies. Those problems are the following: the papers are so old that the methods that were used are now obsolete, the papers don't investigate the salts across a wide enough range of temperatures nor at varying compositions, and finally many of the salts that are seen as candidates today were not given as much attention when molten salt reactors were first conceptualized which has resulted in a lack of research on them. Indeed, the research into these salts is lacking in many ways. This study seeks to investigate a collection of promising coolant salts in depth with acknowledgment to those past studies. LiF-NaF-KF will be used as a calibration standard and for the purpose of verifying our methodology. A multitude of different compositions of NaOH-KOH will be evaluated for their densities and heat capacities. And finally, BeF_2-NaF will be evaluated within the question of if the properties are desirable enough that the dangers posed by beryllium are an acceptable risk. BeF_2-NaF will have melting point, heat capacity, density, and vapor pressure measurements performed. Additionally, extensive impurity analysis and removal was done to our BeF_2-NaF samples.

Table of Contents

List of Figures

List of Tables

List of Abbreviations

ICP-MS Inductively Coupled Plasma Mass Spectrometry

ORNL Oak Ridge National Laboratory

DSC Differential Scanning Calorimetry

MDSC Modulated Differential Scanning Calorimetry

TGA Thermogravimetric Analysis

ICP-OES Inductively coupled plasma-optical emission spectrometry

EDS Energy Dispersive Spectroscopy

SNS Spallation Neutron Source

MSR Molten Salt Reactor

Chapter 1

Introduction

As the field of nuclear engineering forges ever-forward into the next generation of nuclear reactors, a multitude of advanced reactor concepts are being considered. The focus of this study is the molten salt reactor. When it comes to molten salt reactors, detailed research is still required on the eutectic salts that are viable for use. In order for a salt to be used, every property of it must be thoroughly investigated for a range of temperatures even beyond those of operation. In this paper, the heat capacity, melting point, vapor pressure and density of a variety of salts are examined. The salts in question are FLiNaK, NaOH-KOH, and BeF_2-NaF.

1.1 LiF-NaF-KF

When determining which salts are candidates for use as coolant in either nuclear reactors or heat-transfer loops, certain characteristics were examined. They must have chemical stability at high temperature, they must have a melting point that allows the reactor to not have to operate at too-high temperatures, they must not be volatile, and they must be compatible with high-temperature materials that may be used [1]. One salt that fulfills many of these requirements is FLiNaK. As a result of this, FLiNaK has been extensively studied for decades [2], and as a result there are a multitude of sources with data on its thermal properties. As a result of this, it makes for an excellent salt to use for calibration or verification [3]. For our purposes, the melting point, vapor pressure, and density of FLiNaK were measured for the purposes of verifying or calibrating our methods.

1.1.1 Melting Point

As far back as the 1950s and 1970s data has been gathered on the thermal properties of FLiNaK, such as with the initial report on thermal properties of fluoride salts from Oak Ridge National Laboratory [4].

Although research into molten salt reactors did not garner interest at the time, decades later the research was picked up once again such as in D.J. Rogers et al.'s 1982 article [5]. Within this article, it is specified that the melting point, as well as other properties, of FLiNaK of composition 46.5%LiF, 11.5%NaF, and 42%KF were measured using differential scanning calorimetry (DSC). Specifically, the Perkin-Elmer DSC-Model 2 calorimeter was used with the associated software. They performed verifications using indium, tin, and lead as well as KNO_3 and LiCl-KCl. Each component of the FLiNaK that they used was thermally purified in order to minimize moisture. Finally, the melting temperature was found to be 460.5 degrees Celsius at its lowest and 463.6 degrees Celsius at its highest. These values do deviate slightly from their listed expectation of 454 degrees Celsius.

Notably, the method used four decades ago is rather similar to the one that is used today, only with some additional steps as required by the technology at the time. To this day, melting point is often measured using DSC such as in Schorne-Pinto's 2024 report [6] in which they used a Netzsch-Geratebau GmbH 404 F3 Pagasus DSC with additional oxygen gettering rings and customized nickel liners. In addition to using DSC for measurements, inductively coupled plasma-optical emission spectrometry (ICP-OES) was used to confirm that the composition of their salt samples was the desired 46.5%LiF, 11.5%NaF, and 42%KF. The results of their measurements indicated that the melting temperature at its highest was 460.5 degrees Celsius and at its lowest was 458.5 degree Celsius. This is in good agreement with the initial measurements performed by ORNL.

Using the DSC to examine the heat flow curve of a salt is evidently a tried-and-true method for determining the melting point of a salt. As such, it is the method that was used in this paper as well when testing the melting point of FLiNaK, if only for the purpose of verification of our method. In a later section the specifics of our method and materials will be discussed.

1.1.2 Vapor Pressure

The vapor pressure of a salt is another important property that must be thoroughly understood before it is implemented in a reactor. As with the melting point, the vapor pressure of FLiNaK and similar fluoride salts have also undergone extensive research. However, in order to understand the method being used to determine the vapor pressure of our salts, it is important to review the method of vapor pressure measurements across the decades in order to explain our method.

The first source in question is that of Langmuir 1913 [7] which details the process in which the vapor pressure of metallic tungsten is evaluated. Their experimental method included using tungsten lamps. Running voltage through the filaments of these lamps, they measured the initial and final voltages, the initial and final amperes, and the initial and final weights of the tungsten filaments in each lamp. Additionally, they noted the temperature of the lamps and the time that passed over each experiment.

The theory behind their method of measuring the vapor pressure has its roots in the Clausius-Clapeyron formula which relates the vapor pressure and the temperature of a substance. By manipulating that formula using the gas law and the relation between resistance and the cross section of their material, they found a formula with constants that could be measured using their method to relate the evaporation rate and temperature. By plotting the resistance vs. time, they determined those unknown constants and had their desired formula.

Although the materials, level of technology, and measurements were different, the paper [7] provides an excellent example of the core of the theory behind these vapor pressure measurements. That being, by using the Clausius-Clapeyron formula as well as prior established relations such as, in this case, the gas law and the relation between resistance and weight, a function can be created that displays the desired relation between temperature and vapor pressure where any unknowns could be measured according to what experimental setup is being used. With this in mind, let us look at further examples of the manipulation of the Clausius-Clapeyron formula as we step ever-closer to our application of it.

The method used for determining the vapor pressure of select materials in this report is the Knudsen cell effusion method. In practice, a Knudsen cell is often a small crucible with a lid with a small hole in it in which a material is heated over a range of temperatures. This method is an indirect measurement where the weight change is measured and then the vapor pressure is found by using that information and the associated calibration. To that end, Giani et al. 2018 [8] outlines this method beautifully. By manipulating the Clausius-Clapeyron formula in conjunction with the Arrhenius equation (a manipulation that will be explained in detail in the method section of this report), a relationship between the change in weight and the vapor pressure is obtained. Although there are unknowns in this equation, those unknowns are found via an external calibration using a known material. Finally, with the unknowns determined, the weight change of the material of focus can be measured and the vapor pressure can be found.

One application of a similar Knudsen cell effusion method with fluoride salts is shown in Yamawaki et al. 2012[9], in which the Knudsen cell effusion method was used to determine the vapor pressure of lithium fluoride monomer, dimer, and trimer. In this experiment, a tungsten Knudsen cell was attached to a Nuclide 12-90HT high temperature mass spectrometer with silver being used as a standard and the vapor pressure of LiF was measured over 1006-1200K. As this temperature range agrees well with the temperature range in which our FLiNaK samples will be measured, this source was used to externally calibrate our system.

It is important to note that Yamawaki et al. 2012 [9] was not only used because of their use of the Knudsen cell effusion method, but also because this source proved to calibrate our FLiNaK data such that it fit well with other sources that measured the vapor pressure of FLiNaK. In order to come to that conclusion, Yamawaki et al. 2012 [9] was compared to three other sources for the vapor pressure of LiF: Hildenbrand et al. 1964 [10], Scheffee and Margrave 1959 [11], and Eisenstadt et al. 1958 [12] by extension. Notably, these sources did not use the Knudsen cell effusion method. Instead, [10] used a torsion-effusion apparatus and [11] and [12] both used a molecular beam method which consisted of a velocity selector, a molybdenum oven, and a detector. With this comparison of sources and methods, and the selection of a calibration material, we can now move onto direct examples of FLiNaK vapor pressure measurements.

The first example of note in the measurement of the vapor pressure of FLiNaK is the technical report of Oak Ridge National Laboratory (ORNL) by McMurray et al. 2020 [13]. In that report, FLiNaK is used for much the same reason as in this report. That is to say, they noted that their use of FLiNaK was meant to simulate how a system would react to similar fluoride salts such as FLiBe. FLiBe, after all, is a very dangerous material to work with, and so it is valuable to have a material such as FLiNaK which can provide a basic guideline of what to expect from the salt. In order to evaluate the uncertainty and functionality of their setup, the researchers of ORNL used a Netzsch STA 409 CD 403/5/G STA-MS Skimmer Coupling System (Skimmer) to measure the vapor pressure of their standard samples of salt. In doing so, they were employing mass spectroscopy and the Knudsen cell effusion method. This example displays that our method of using FLiNaK to test our machinery and setup is one that is well accepted by industry.

The next example of the measurement of the vapor pressure of FLiNaK is that of Y.S. Choi et al.'s 2013 report [14] which sought to explore the vapor of FLiNaK in the context of its interactions with plasma. With this specific goal in mind, their setup is different, but the idea of their method is still the same. Though they used Energy Dispersive Spectroscopy (EDS) to analyze the plasma interaction with

FLiNaK, the Knudsen cell effusion relation is still what was used to determine the vapor pressure. For, though their setup also included a silicon sample upon which was deposited the vapor, the FLiNaK was still in a Knudsen cell, a crucible with a hole in its lid. Though the desired data is quite different, still a similar method is used.

Another example of this method is that of M. Yamawaki et al.'s 2015 article [9] in which vaporization behavior of fluoride salts was examined in order to better understand the hypothetical case of a severe fuel pipe break. In this study, a quadrupole mass spectrometer (Pfieffer Vacuum QMG700) was used with a tungsten Knudsen cell. The salts they focused on were that of LiF, LiI, and CsF. Vapor pressure in this case was measured using the measurement of the intensity of the ionic current. This method was used because of their desire to focus on the specific vapor species that resulted from the vaporization of each fluoride salt.

All of these examples are to say that the method of mass spectrometry in conjunction with the Knudsen cell effusion method is a tried and true method for the measurement of the vapor pressure. Not only that, it offers versatility in the types of data that can be gathered, be it data concerning the relation between a salts mass change and vapor pressure, or perhaps the relation between the ionic current intensity and the partial vapor pressure. This experimental setup is decidedly reliable and worth using with FLiNaK in order to establish this setup for use with other salts of interest.

In addition to the experimental methods of determining vapor pressure, there are also methods of deriving what the vapor pressure may be prior to experimentation. This modeling work is instrumental in understanding the validity of a measurement, and so our data will be compared to such theoretical functions of vapor pressure. One such source which displays modeling of the vapor pressure of FLiNaK is that of J. Schorne-Pinto et al. 2024 [6] in which they used the MQMQA model to plot the vapor pressure. They also used thermodynamic functions of equilibrium partial and total vapor pressure over a FLiNaK melt in their plot.

1.1.3 Heat Capacity

A high heat capacity of a salt is desirable because a material with a high heat capacity can store large amounts of heat without changing temperature drastically. For that reason, the heat capacity of many candidate salts is measured. FLiNaK, as mentioned prior, is one of the most researched salts within the area of molten salt research.

One study, [5], was mentioned prior in reference to the studies measurements of FLiNaK's melting point. Using their same DSC setup as for the melting point, they measured the heat capacity with a few additional steps. That being, they took extra precautions in preparing the samples for measurement. Their sample pans were hermetically sealed and were cycled through melting and then cooling multiple times to condition their samples.

A more recent example of this measurement being performed is in [15] where they also used DSC to measure the heat capacity. In this study, FLiNaK was used as a standard in their process of measuring the heat capacity of their target salts. First, they calibrated their system using pure salt standards to an accuracy of (+/- 5%) for heat capacity. They used a heating rate of 10K/min, argon for their atmosphere,

and a Pt-Rh alloy crucible with a perforated lid. Their process involved the measurement of their empty crucibles as a base, then the measurement of their standard (FLiNaK), and finally they measured their test sample. This study is an excellent example of the accepted use of FLiNaK as a standard for these types of measurements.

Both studies include the use of DSC to measure the heat capacity. This method has been used and further developed for decades. However, it is not perfect. In fact, an improved version of DSC, modulated differential calorimetry (MDSC), has been accepted to be a more accurate way to determine the heat capacity. Though the method is more complex, the technology of today makes it much easier to do than it was years ago. For this reason, studies like [3] opt for MDSC instead of just DSC.

1.1.4 Density

Another property necessary for consideration of a salt being used is the density. Density is significant for the purpose of understanding the heat transport capability of a salt in forced and natural convection [2]. Because of this, it is a common set of data to collect when researching a material, salt or not, to be considered for use in a nuclear reactor.

As with any property of a material, there are many ways to measure it. An article by R.C. Gallagher et al. [16], in which they measured the density of FLiNaK, displays a method called the Archimedean method, a common method for determining the densities of liquids and salts, in which the displacement of a fluid aids in the determination of the density. The density can be found in this way by relating how much a fluid displaces from a known solid plummet to the density of that fluid (taking into consideration things such as the temperature and surface tension). In addition to their experimental collection of data, they also proposed that, in order to provide data that is compelling and trustworthy, an analysis of the density of FLiNaK via modeling is also necessary. As a result, they used a model which included RK expansion to estimate their density.

Another experimental technique is that of neutron radiography. One example of this technique is in an article by A.M. Long et al. 2021 [17]. With this technique, the density measurements are done remotely by accessing a spallation neutron source (SNS). The SNS is used to supply neutrons which are, in simple terms, then guided on a path that passes through the molten salt samples. After passing through the samples, the beam is then imaged using a neutron imaging setup. Because of the complexity and difficulty in procuring the needed allowances for access to such a setup, this experimental technique was discarded.

In addition to the experimental techniques of determining the density of a material, there are also models that can be used. For example, a 2009 article by Salanne et al. [18] details their use of a model to display how density can be extrapolated with the goal of modeling other properties as well. In their model, they used a first principles procedure which allows for only the density to come into consideration. This allowed them to then determine the interaction potentials for the molecular dynamics of the system. Their system involved the use of fluoride salts. Although modeling is useful, it is often deemed necessary to experimentally procure the desired density data.

With those methods outlined, [19] provides an example of FLiNaK's density being measured using the Archimedean method. In their setup, a shaft furnace was used in which the sample was lowered from the top along with electrodes that were used to confirm the melted status of the salt. The depth of those electrodes' immersion was controlled via electrical contact. With their recorded volume and mass of their samples, their setup automatically recorded the density every 3s of their temperature intervals. Their setup did these calculations by using a set of equations which relate the mole fraction, molar volume, concentration, and density to one another. This study paid special attention to the concentration due to their focus on the effects of adding select materials into their FLiNaK melts. This setup, while useful for their purposes of adding additional materials later in their process, could benefit from greater control over their system. Additionally, they did not mention the possibility of bubbles forming within their melts, a known problem for this type of measurement. For that reason, this method cannot be used precisely. However, it is still a good example of the Archimedean method.

A much older example of FLiNaK's density being measured is seen in the 1958 study [15] where they used a method similar to the Archimedean method. For their density measurements, the liquid salt samples were weighed with a plummet suspended within the mixture. Little further detail is listed within this source, but it is not unreasonable to assume that their equipment was not as reliable as today's equipment is. Still, [15] is a representation of the Archimedean method having been used for decades in many different forms.

In this study, FLiNaK is used as a calibration material for the density calculations of our FNaBe samples. These calibration curves are taken directly from J. Park's article [3] because the exact same setup from the exact same lab was used for the density measurements of this report. Further details on these density measurements will be detailed later in this report.

1.2 NaOH-KOH

1.2.1 Melting Point

The melting point of NaOH-KOH is well studied. The following Figure 1 displays the phase diagram of NaOH-KOH [20].

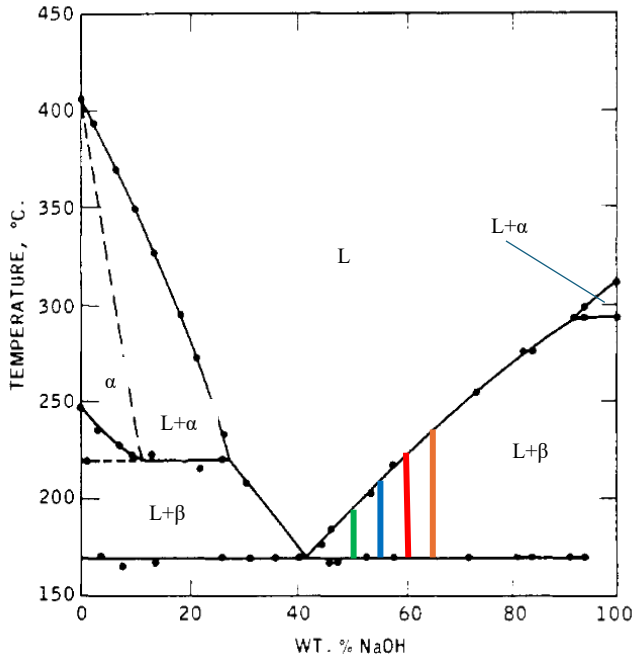

Figure 1. Solid-liquid equilibrium in the KOH-NaOH system

Figure 1: The phase diagram of the NaOH-KOH system as taken from [20] with the melting point labeled for the equimolar composition in green, 0.55-0.6 in blue, 0.6-0.4 in red, and 0.65-0.35 in orange.

The 1964 study, [20], was performed with the goal of understanding NaOH-KOH as a solvent. As a result of the salts high absorption of water, they had to heat their NaOH sample for 24 hours and their KOH sample for 6 hours before combining the two into their eutectic mixture. Their measurements were performed by placing a larger batch, 50g, of the hydroxide mixture into an aluminum cylinder and then using a furnace to melt and regulate the rate of cooling. To create the phase diagram, Figure 1, they used cooling curves rather than heating curves. They noted that their salt samples, if high in water content, would attack the aluminum containers, but if the water was dried out then the salt did not attack the container as voraciously. To measure their data, they used a thermocouple immersed into the melt.

A far more recent study, [21], used TGA/DSC analysis to examine the thermal behavior of NaOH-KOH. They produced heat flow curves of the NaOH-KOH mixture and noted that there were two peaks present. One peak represents water evaporation and the other represents the true eutectic point of the mixture. This study observed those curves for a range of mole ratios of NaOH to KOH, a valuable endeavor on their part as most studies tend to focus on the 1:1 mole ratio. Upon evaluating 0:10, 1:9, 3:7, 1:1. 7:3, 9:1, and 10:0 mole ratios heat flow curves, they found that the 1:1 ratio had the most desirable, the lowest, eutectic point. As such, the 1:1 ratio was used for all of their remaining measurements.

For this study, measuring the melting point of NaOH-KOH was not performed. However, such data as in [21] is valuable for considering the behavior of the salt during our measurements.

1.2.2 Vapor Pressure

One of the properties of NaOH-KOH that has seen less research is that of the vapor pressure of the salt. However, the base component salts have seen some measurements done of their vapor pressure. One study, [22], employed a dynamic method for measuring the vapor pressure of potassium compounds. This is due to them not finding an effective gastight material that would not be corroded by their chosen compounds at high temperatures. This dynamic method that they chose involved passing a volume of gas over the substance whose vapor pressure is being measured. By determining the loss of weight and observing the saturation of the gas as it passes over the substance, partial pressures can be determined. This technique, while appropriate in 1920 when this study came out, is quite outdated today. These days the gastight material that they were missing isn't so difficult to procure.

One study that was performed in 1967 [23] created a complex setup with which they found the vapor pressure of their NaOH at three set temperatures. This setup involved a series of tubing which led pure dry N2 into a furnace in which the NaOH was being held and monitored using thermocouples. Another series of tubes then took the output gas which was introduced to a drying agent before ending in a gas collecting cylinder. Their NaOH samples, by design, had a 0.8% water content if only to have a repeatable starting point. After the measurement, steps were taken to evaluate the contribution of water to the vapor pressures that they measured. This study is a step towards a more reliable method of vapor pressure measurements, but it does not compare to the systems designed today.

A 1981 study, [24], lists the thermal properties, including vapor pressure, of a wide range of salts. This includes NaOH and KOH separately. It is noted that the method used to make the measurements of those vapor pressures was via the Knudsen cell effusion method and boiling point methods respectively, but the specific setup is not listed. Notably, in conjunction with the given data for NaOH, they also noted the dangers that the salt posed. It was noted that the salt was prone to keeping water trapped within it. At high temperatures, this may cause pressure to

build as air is trapped from the steam generated. Additionally, as the temperatures increase, that steam can become especially dangerous and react with the caustic solution. Such dangers also applied to KOH. This note further exemplifies the significance of minimizing the water present within the mixture of the two. For whatever short time the salt may be exposed to air, it may absorb water, and then at the higher temperatures of the vapor pressure measurements, that releasing of steam may lead to error.

It is likely for those very reasons above that so little research has been done into the vapor pressure of NaOH-KOH specifically. It is also because of that volatility that it must be evaluated. However, this study did not make such measurements.

1.2.3 Heat Capacity

NaOH-KOH, as well as other hydroxide salts, is highly diverse in its applications [24]. Yes, they can be used in nuclear reactors, but they also have high potential for usage for energy storage in a number of systems. This is because of the highly desirable heat capacity of these salts which trend towards being quite high.

All the way back in the 1980s, NaOH-KOH eutectic has been evaluated for its heat-thermal storage capabilities. One example of this experimentation is in Takahashi, et al. (1987) [25], in which NaOH-KOH (50-50 mol%) was evaluated over the temperature range of 330-575K in comparison with NaOH and LiOH-NaOH. The purpose of this paper was to determine if these eutectic mixtures were indeed viable materials for use in latent heat-thermal energy storage equipment which was to be operated at around 440K to 490K.

The method that was used was that of dynamic scattering calorimetry (DSC), which was relatively new at the time (1987). They noted that the specific model used was that of the Perkin-Elmer DSC (type II). Measurements were conducted under nitrogen flow and at heating and cooling rates of 5 K per minute. Calibrations were performed using a synthetic sapphire disk of 27.87mg. The crucible that they used was made in-lab out of polytetrafluoroethylene due to hydroxides corroding aluminum, platinum, and quartz (the more traditional crucible materials).

Within their data, they did note that there was a notable deviation between 360-365K which is due to a peak formed by water contamination due to the highly hygroscopic nature of the KOH.

Another source that uses DSC in order to evaluate the heat capacity of NaOH-KOH is found within an article by Y.M. Baikov, 2009 [26]. In this experimental setup, a similar process is used in which they measured the heat capacity using DSC from ~300K to ~450K with the context of their desired data relating to electrolytic mixtures involving the hydroxide salt. They evaluated their data over a temperature range of 10-1.25K/min and they used white sapphire as a calibration material. Their salt mixture was that of an equimolar NaOH-KOH eutectic. Within the heat flow curves obtained using their DSC, they noted anomalies/hysteresis with a magnitude of 5-7K that increase with increased scan rate. With this in mind, they extrapolated their data to a scanning rate of zero with the desire to make the data as consistent and anomaly free as possible. Although our own method did not include extrapolation towards zero, the scan rate used was made as small as possible for this very reason.

As valuable as such sources as [25] and [26] are, they are lacking in a few ways. One point in which they are lacking is that they do not experiment on eutectic mixtures of differing mol percentages.

Both sources focus purely on an equimolar composition and do not investigate other compositions. This is understandable considering the focus of their papers was not to purely investigate NaOH-KOH eutectic, but that does not absolve the lack of detailed experimentation on the matter.

Another point of contention is that of the temperature range over which the measurements were performed. Although the temperatures that the experiments of [25] and [26] were performed over were valuable to their specific application, there is a distinct lack of data for temperatures higher than 575K. Of course, in the context of nuclear reactors, the behavior of a material at higher temperatures must be understood.

Finally, these papers, as well as many reports on heat capacity measurements, describe the use of DSC rather than MDSC.

Modulated differential scanning calorimetry (MDSC) is a method that has been used for decades to measure the heat capacity of materials [27]. It is a method that allows for a more detailed and trustworthy examination of heat capacity, as will be discussed in more detail later. As such, this tried-and-true method will be used in this report to measure the heat capacity of our chosen salt.

The data collected for the heat capacity of the NaOH-KOH salt was also compared to the NIST data of NaOH and KOH [28].

1.2.4 Density

An article by S. Dai, et al. [21] provides an example of density measurements being performed with NaOH-KOH. Within this article, the measurements were most similar to the Archimedes technique. They used a Westphal balance to lower a plummet into their NaOH-KOH mixture at 673K. According to their specific goals of examining the destruction of organochlorine in the NaOH-KOH, additional machines were added to their system. Although there were those additional machines and added steps, the idea remains the same, that being that in the lowering or raising of the plummet, the density can be calculated from the resulting weight and height data.

Again, the examples of density measurements of experiments done by other groups are a bit lacking for our own purposes. In order to truly understand NaOH-KOH eutectic, we examined the density of a multitude of compositions at larger range of temperatures. Additionally, a technique based on the Archimedes method was used for our mesurements. This method is explained at length in [3], and will be explained in some detail within the methods section.

As a part of our technique, calibration measurements were performed using FLiNaK or NaOH as a basis due to the extensive research already done on the materials at a large range of temperatures. The desired density-temperature correlations that were used in order to form the calibrations using those materials are seen in [3] for FLiNaK and in [29] for NaOH. Further details on the technique used for measuring the density and forming the calibration curves will be outlined in the methods section.

1.3 BeF_2-NaF

1.3.1 Melting Point

Another necessary and simple measurement to be done is the melting point. As mentioned in the FLiNaK section, many sources that measure the melting point of the salt use DSC to do so. It is much the same for BeF_2-NaF where [30] provides a comparison between modeling using first principles molecular dynamics and DSC experiments on BeF_2-NaF. With this comparison they delved into the specific structure of the salt molecule as it is increased in volume and or temperature. Due to how promising BeF_2-NaF is as a candidate for use in multiple molten salt systems, it is expected for more extensive work to be done into the modeling and experiments on the salt. However, for this paper only the experimental side of the issue is considered other than some minor comparison between expected and experimental values.

1.3.2 Vapor Pressure

The vapor pressure for BeF_2-NaF can follow the technique that has been mentioned prior: the Knudsen cell effusion method and mass spectroscopy. Just as LiF was used as the calibration material for FLiNaK measurements in conjunction with the data from [9], LiF can also be used to calibrate the system for BeF_2-NaF measurements due to all salts involved being fluoride salts. However, other articles have displayed different techniques in which the vapor pressure of BeF_2-NaF was measured.

An article by Sense and Stone [31] measured the vapor pressure of a collection of fluoride salts, including BeF_2-NaF. Their method involved collecting the condensation of a salt and consequently measuring the amount of salt that condensed and the composition. Though this method can be effective, using TGA/DSC is far simpler and has been widely used to measure the vapor pressure of a variety of salts.

1.3.3 Heat Capacity

The measurements performed for BeF_2-NaF follow the same procedure as for NaOH-KOH and FLiNaK. Modulated DSC was used for the desired temperature ranges for the salt, but as the procedure was less polished at the time, it was a bit different from how the measurements were done for NaOH-KOH, to be outlined in a later section.

As with the other salts, a review will be done of the methodology of other sources in their measurements of the heat capacity of fluoride salts, particularly BeF_2-NaF, in order to examine the precedent, set on the topic.

Our first source is that of S.I. Cohen et al. 1956 [32] which uses calorimetry, but in a far less polished sense in which they simply dropped the samples of the salt into an ice or copper block-based calorimeter. This was done to measure the heat capacity of a variety of salts, including BeF_2-NaF. However, the procedure used for these experiments is archaic compared to the machinery that researchers

have access to today. Still, this represents an earlier form of the same experiments that are being done today in order to measure the heat capacity Yes, they did not have access to machines that allowed for DSC or MDSC, but they still measured the heat released by their samples according to their systems. One might even say this is the precursor to the DSC method in which the software associated ends up displaying the heat flow curve.

This method, which has been improved over decades, is consistently used today. Most sources list the use of either DSC or MDSC in their measurements of the heat capacity. For example, articles from Redkin et al. [33] and Rogers et al [5] (mentioned in a prior section) use DSC to measure the heat capacities of FLiBe and FLiNaK respectively. Then D'Aguanno et al. displays measurements using the more advanced technique of MDSC [34] to determine the heat capacities of KNO3 and NaNO3.

Experimental procedures are not the only way in which the heat capacity has been found. Analytical calculations can also be done to find the heat capacity and can be quite useful for comparison with the experimental data. The method most relevant to this paper is that of the ideal-mixture method. In this method, the linear summation is taken of the mass fraction weighted heat capacities of each component of the material in question [35].

1.3.4 Density

Just as outlined for NaOH-KOH, the density system that was used for our experimentation was the exact same as in [3]. Where the density measurements of NaOH-KOH required a new set of calibration curves, the density measurements for BeF_2-NaF use the exact same calibration curves made using FLiNaK in [3]

As noted in [36], [37] displays an extensive set of thermal property data, including the density of a large number of fluoride salts including BeF_2-NaF. However, as is often the case with the initial studies on molten salt, the methods from all those decades ago are unreliable compared to the advancements made in technology today. The data is not without its merit since it allows an opportunity for comparison. However, [36] offered a different perspective on determining the density of a material. Instead of performing measurements with the notoriously toxic BeF_2-NaF, they instead opted for the modeling of these materials using first principles molecular dynamics. Still, despite this valuable approach, it is important to investigate a topic in both theory and experimentally. And so, this paper seeks to focus on the experimental side of density measurements of BeF_2-NaF.

1.3.5 Salt Purification

The final point of note in regard to the experimentation with BeF_2-NaF is the salt needing to be purified due to oxygen contamination during the process of fixing the salts composition. The process by which the salt was purified was through an HF gas purification system. [38] displays one example of the theory behind the system, where NH4HF2 was used to both convert UO2 and ThO2 into anhydrous tetrafluorides and remove the oxide impurities. Another example of this idea being used is [39] in which HF gas is used instead for the same reaction of fluorination of oxides. The idea is HF gas will react with

the oxygen and result in products that can be removed from the container through a flow of gas going through the purification system. In this way, the impurities can be removed from the mixture and the salt can be quenched or samples taken. This procedure is outlined in [40] and [41], reports by ORNL that detail the procedure for handing the molten salts in question. Within these reports are the details of the system of using HF-H_2 gas to purify salts which they developed.

1.4 The scope of the present study

With the above literature review considered, now the focus of this study will be outlined. FLiNaK will be used as a calibration and verification material. It's melting temperature and vapor pressure were measured to that end. Our BeF_2-NaF data is far more extensive. The melting temperature, density, vapor pressure, heat capacity, and even the impurity levels were all measured. Finally, the NaOH-KOH had its density and heat capacity measured for four compositions. This all is outlined in Table 1.

Table 1: A summary of the properties of focus for this study.

Salt	**Density**	**Vapor pressure**	**Heat capacity**	**Melting temperature**
FLiNaK		Measured		Measured
BeF_2-NaF	Measured	Measured	Measured	Measured
NaOH-KOH	Measured		Measured	

Chapter 2

Method

2.1 Melting Point

The method used to determine the melting point of a salt sample involves using a DSC to create a heat-flow curve across a set of temperatures meant to encompass the expected or predicted melting point of the salt. Per sample, there are three curves that are generated. Each curve is done at a different heating rate. One is 15 C/min, the next is 3 C/min, and the last is 1 C/min. Upon acquiring the heat flow curves, the software connected to the DSC can then allow the user to determine the onset temperature (T_{onset}) and the peak temperature (T_{peak}). T_{onset} then represents the melting point of the salt.

However, there are some instances in which the heat flow curve presents two separate peaks. This is the case for the BeF2-NaF measurements of this study. In the case of two separate peaks, the T_{peak} of the second peak represents the melting point. This is because the first peak represents the eutectic point in which there is liquid as well as crystals of both components of the salt. The second peak represents the liquidus of the salt, the true melting point.

2.2 Heat Capacity

The heat capacity can also be measured using DSC. Specifically, in this report, MDSC is used for greater accuracy of the data gathered. Where DSC offers measurements via a linear heating and cooling rate, MDSC measures the heat capacity by adding a sinusoidal oscillation around that linear heating. Because of this sinusoidal oscillation, this creates a quasi-isothermal condition which allows for greater accuracy than for DSC.

With the temperature sinusoidal, the heat capacity can be expressed with Equation 1,

$$\frac{dH}{dt} = C_p \frac{dT}{dt} + f(T,\ t)$$

Where $\frac{dH}{dt}$ is the total heat flow of the linear heating rate (equivalent to standard DSC), C_p is the heat capacity calculated from the heat flow corresponding to the modulated heating rate, $\frac{dT}{dt}$ is the heating rate, and $f(T,\ t)$ is the kinetic component of the total heat flow [27].

2.3 Vapor Pressure

To measure the vapor pressure, the Knudsen Cell Effusion method was employed. The best description of this method starts with Figure 2,

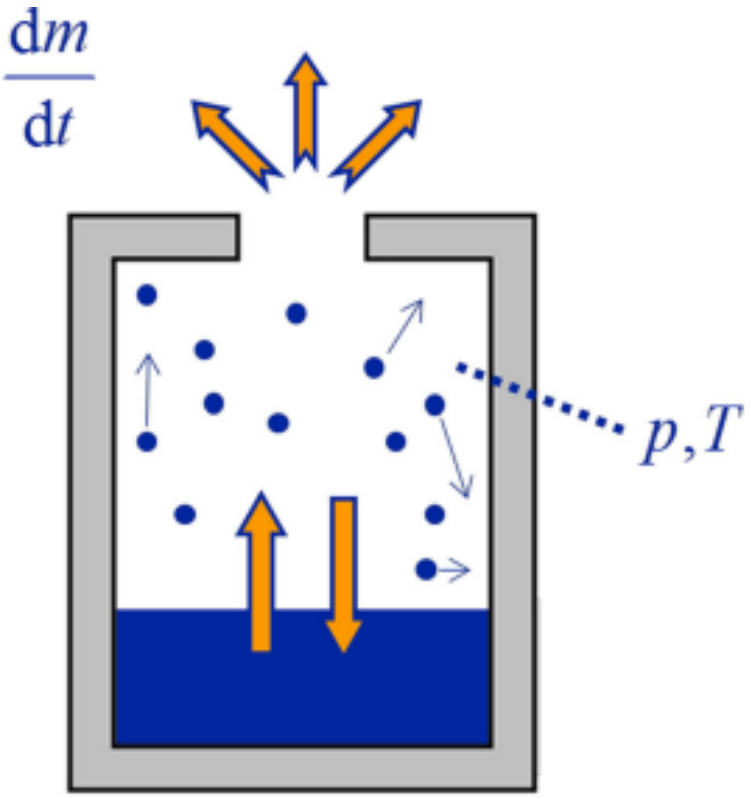

Figure 2: A graphic of a Knudsen effusion cell, taken from [8]. A crucible with a small hole in its lid through which vapors flow out.

Which displays the definition of a Knudsen effusion cell. The Knudsen Cell itself creates an environment in which the pressure is at equilibrium. The hole in the lid allows a surface from which that equilibrium is achieved. In our case, the cell creates the conditions for a flow out of that hole. The weight change is measured by the TGA machine. With these conditions, following the definition of the vapor pressure, the weight change can be related to the vapor pressure. As the salt melts sits uniformly at the bottom of the crucible. The vapor then proceeds to be released of a measurable amount in the change of weight over time of the sample. By using thermogravimetric analysis (TGA), that weight change can be measured which is then used in the determination of the vapor pressure through external calculation.

The calculation of the vapor pressure begins with the Clausius-Clapeyron relation,

$$\ln(p) = L - \frac{\Delta H}{RT}$$

Where p is the vapor pressure, L is the latent heat, ΔH is the change in enthalpy, R is the ideal gas constant, and T is the absolute temperature.

Then is the Arrhenius equation, which is as follows,

$$\left|\frac{dm}{dt}\right| = a * \exp\left(-\frac{b}{T}\right)$$

Where dm/dt is the weight change, a and b are constants, and T is the temperature. By combining the Clausius-Clapeyron equation with the Arrhenius equation, the following equation can be found,

$$\log(p) = c * \log\left(\left|\frac{dm}{dt}\right|\right) + d$$

Which presents the desired relation between p, the vapor pressure, and dm/dt, the change in mass. The change in mass can be measured using TGA which then allows the vapor pressure to be solved for. The constants, c and d, are found through external calibration. The calibration material, which has a known vapor pressure, is put into the DSC/TGA and its mass change measured over the desired temperature range. Then the vapor pressure and the mass change can be plotted against one another in a logarithmic plot to find c and d. Once c and d are found, then the desired material can be put into the DSC/TGA, the mass change measured, and then the vapor pressure solved for. For reference, this exact procedure is outlined in [8].

2.4 Density

Although the system used for measuring the density of our molten salts was similar in nature to the Archimedean method, which is based around the displacement of a fluid by a known plummet, it is not precisely the same. Instead, the system used is that of the system outlined in [42]. After all, the measurements done in this paper were performed in the exact same laboratory setting.

The system in question is based around the measurement of the height of the molten salt at different temperatures. By pre-establishing the dimensions of the crucible that is being used, the height can be used to determine the volume of the salt at each temperature. That combined with the mass of the salt before and after the measurements allows the density of the salt to be calculated using the simple relationship between the mass, volume, and density.

Figure 3, taken from [3], displays the system's setup,

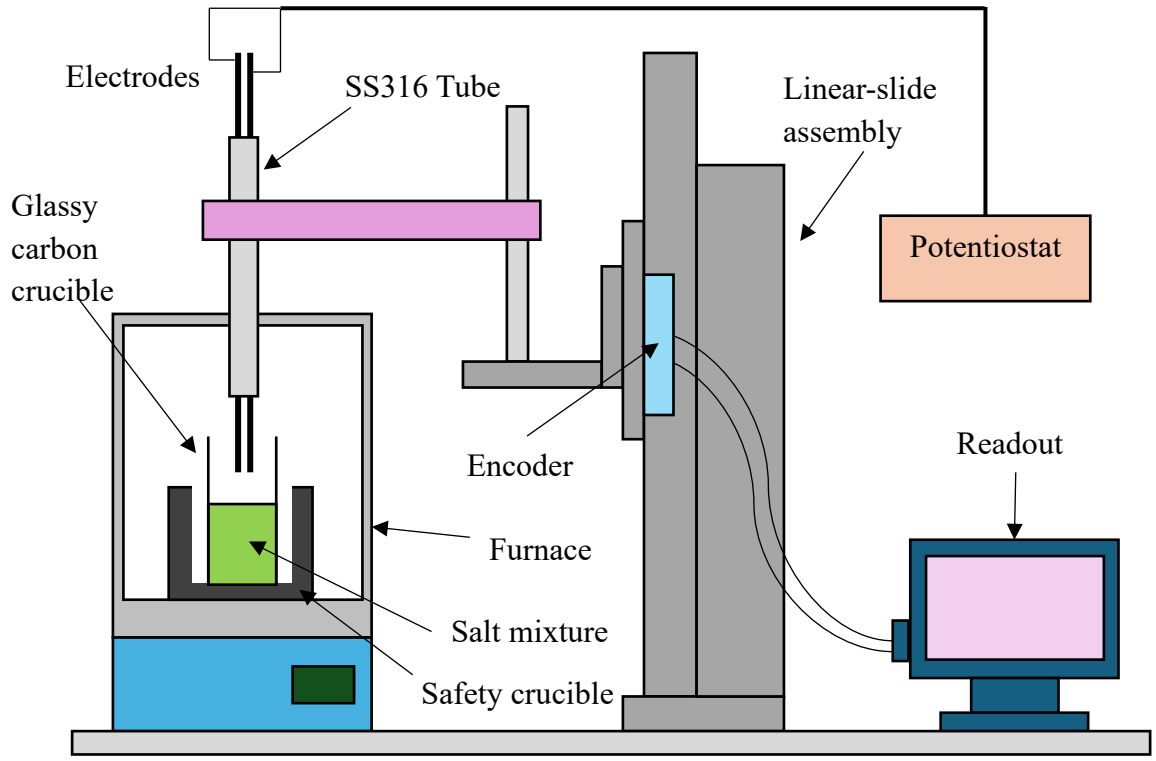

Figure 3: A graphic displaying the density measurement system as taken from [3].

The setup of this system includes the furnace, the crucible of known dimensions that holds the salt, the linear-slide assembly which raises and lowers the electrodes and displays the height, and then the electrodes themselves which are connect to a potentiostat. The system measures the height of the salt through the manual lowering of the electrodes. The potentiostat displays when the electrodes come into contact with the surface of the molten salt through the change of open circuit potential. The linear-slide assembly shows the associated height at that point through the readout.

Then, once those heights are noted, the density can be calculated with the known data and calibrations. Those calibrations are the volume-height correlations and, as the name implies, allow the volume to be calculated given the measured height. Some of the necessary calibrations were from [3] which were made using FLiNaK.

However, since these calibrations only work for fluoride salts, the hydroxide salts whose densities were measured required a new set of calibrations using NaOH.

As mentioned in a prior section, ideal-mixture calculations can be performed to provide a comparison for the measured density. In order to make those calculations, the density temperature correlations for the associated components of the salt must be known. The relevant density temperature correlations are in Table 2,

Table 2: A table of the relevant materials of this work and their density-temperature correlations for the purposes of ideal-mixture density calculation.

Materials	Temperature Range, C	$\rho\ [\mathrm{g/cm^3}] - T\ [C]$ Correlation	Reference
LiF	866.8-1036.8	$\rho = 2.3581 - 0.4902 \times 10^{-3}T$	[43]
NaF	996.8-1146.8	$\rho = 2.655 - 0.540 \times 10^{-3}T$	[43]
KF	856.8-1016.8	$\rho = 2.6464 - 0.6515 \times 10^{-3}T$	[43]
BeF_2	799.8-849.8	$\rho = 1.972 - 1.450 \times 10^{-5}T$	[37]
NaOH	399.8-799.8	$\rho = 2038.16 - 0.489T$	[29]

2.5 Salt Purification

The details of the salt purification system, which removes oxides, sulfides, hydroxides, and structural metal impurities, are based upon the following reactions [3],

$$O^{2-} + 2HF_{(g)} \rightleftarrows H_2O_{(g)} + 2F^-$$

$$2OH^- + 2HF_{(g)} \rightleftarrows H_2O_{(g)} + 2F^-$$

$$S^{2-} + 2HF_{(g)} \rightleftarrows H_2S_{(g)} + 2F^-$$

$$MF_x + \frac{x}{2}H_{2(g)} \rightleftarrows M^0 + xHF_{(g)}$$

With these reactions in mind, the purification system was developed which is comprised of a many hour long, multi-stage system of the following basic steps: purging with the carrier gas (argon), purging with HF-H_2, then purging with argon once again.

A simplified version of that system is outlined in Figure 4 which was created in the nuclear materials and fuel cycle lab by one of its members,

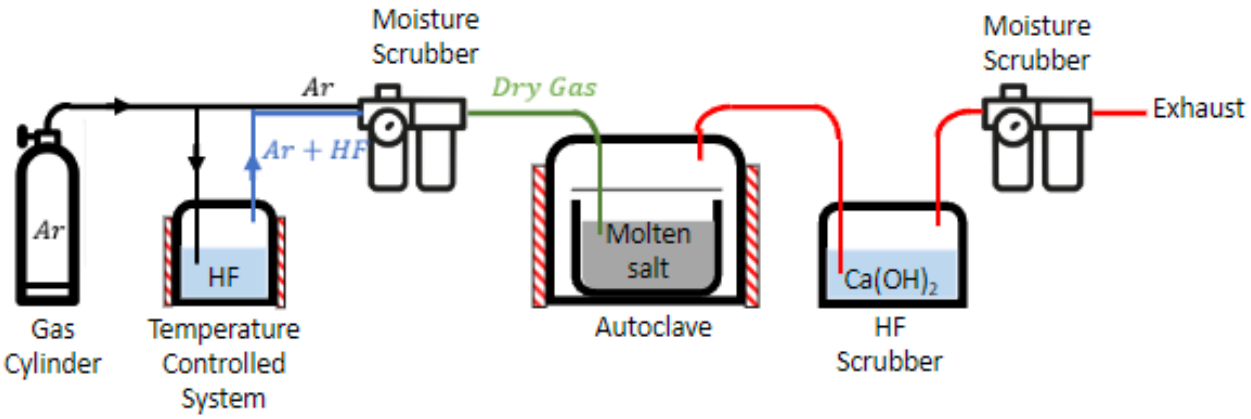

Figure 4: A simplified diagram depicting the HF based salt purification system. This image is taken from the SOP of the Nuclear Materials and Fuel Cycle Center and was made by Dr. Amanda Leong.

Chapter 3

Experiment

3.1 FLiNaK

3.1.1 Materials

The FLiNaK used was created in the nuclear materials and fuel cycle center. In reflection of the other studies which have used FLiNaK in their research, the LiF-NaF-KF of this study had the composition of (46.5-11.5-42.0 mol%).

As the lab did not have the OH and CS systems fully installed at the time, the samples of FLiNaK did not have impurity analysis done on them. However, as the FLiNaK data was gathered more for a testing of the system than anything else, this is acceptable.

3.1.2 Melting Point

Measuring the melting point of FLiNaK was a very straightforward process. A sample of FLiNaK between 30-35mg was measured out and placed into the sample pan. Then, the sample was heated to 60 degrees Celsius above the expected melting point and then 60 degrees below the melting point. This created the heat flow curve from which the T_{onset}, the melting point, could be found.

Before the measurements themselves were taken, calibrations were performed using the calibration system inherent to the DSC. This system uses Zinc, Aluminum, and Silver as standards for calibration. Upon the DSC determining that the calibration was successful, that the results were within <1% of the accepted value, the measurements could proceed.

3.1.3 Vapor Pressure

The vapor pressure measurement of FLiNaK starts with the measurement of the calibration material. The calibration material, LiF, was measured over the temperature range of 850C to 1090C. Every 10-20 degrees of increase, the temperature was set to maintain that temperature step for ten minutes. The weight change was observed and recorded over that time. Because LiF is the calibration material, its vapor pressure is known and can be plotted against the weight change to form the calibration curve in Figure 5.

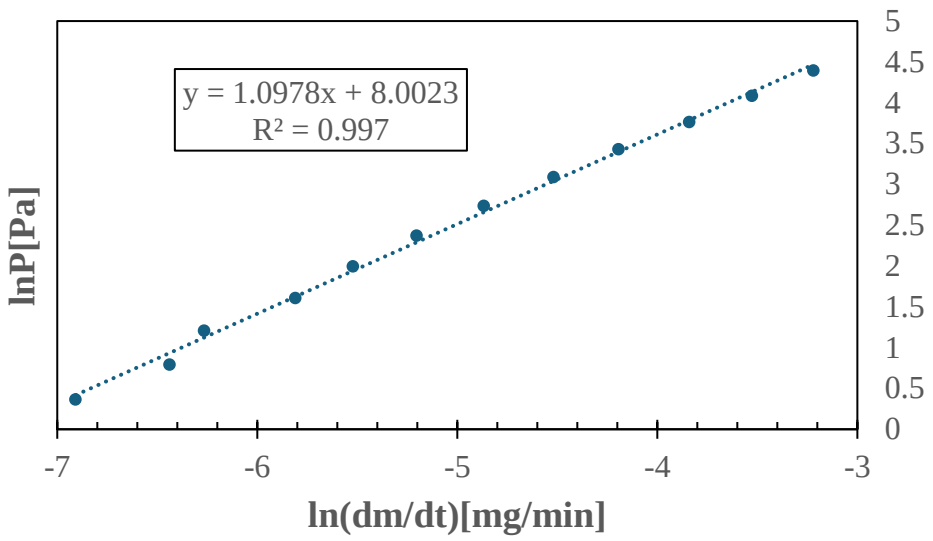

Figure 5: An LiF calibration curve used for the vapor pressure emasurements of FLiNaK.

With this calibration curve obtained, the measurement of FLiNaK, following those same steps, could proceed. By taking the slope and y-intercept from the calibration curve, the vapor pressure can be found by using the gathered weight change data.

3.2 NaOH-KOH

3.2.1 Materials

The materials used for the experiments performed on the NaOH-KOH salt samples are the following four compositions of salt of Table 3,

Table 3: The set of NaOH-KOH samples and their respective compositions in mol%.

Sample number	NaOH mol%	KOH mol%
16	0.5	0.5
17	0.55	0.45
18	0.6	0.4
19	0.65	0.35

For the calibration of the heat capacity system, synthetic sapphire was used for most measurements. However, before synthetic sapphire was used for all of the calibrations, NaF was used instead. For the calibration of the density system, NaOH was used.

All experiments performed on NaOH-KOH were done using glassy carbon crucibles due to them not reacting with the salt as well as their displayed stability over the temperature ranges of interest.

3.2.2 Heat Capacity

Prior to any measurements being conducted, both internal and external calibrations were performed. The internal calibration was done using synthetic sapphire. The external calibration was initially done with NaF, but this was changed to synthetic sapphire after the first set of data was gathered and NaF displayed a lack of consistency. The external calibration data was normalized using the NIST data for either sapphire [44] or NaF [28] to obtain a calibration factor that was applied to the NaOH-KOH data. Both internal and external calibrations were performed before each measurement to ensure that the data is as reliable as possible.

Between each measurement, the beams and the crucibles were cleaned. The beams were initially cleaned using air, but this was later changed to argon. This change was made upon discovering how harmful the air cleaning was to the beams. The crucibles were cleaned thoroughly by cleaning them twice in an ultrasonic machine using DI water, then once within the DSC using argon.

After the calibration of the system, the cp measurements of the salt sample can then proceed. Each sample is melted down before heat capacity measurements are performed. Each type of salt is measured three times. Those three measurements are then averaged. Certain datasets; however, had outliers that were not used for averaging.

This procedure was applied to the four different compositions of NaOH-KOH salt listed in Table 3.

3.2.3 Density

The process of creating the calibration curves for use in this system involves measuring the height of a known material at different weights across a range of temperatures. For example, when the NaOH calibration curves were created, masses of 4g-6.5g were used to make measurements across the temperatures of 350-600C. The resulting volume-height correlations are in Table 4,

Table 4: NaOH volume-height calibration curve equations for the purpose of the measurement of the density of NaOH-KOH.

NaOH Volume-Height Calibration	
Temperature (C)	Volume-Height Curve
350	V=0.079*h+0.23
400	V=0.079*h+0.22
450	V=0.079*h+0.23
500	V=0.079*h+0.22
550	V=0.079*h+0.22
600	V=0.079h+0.22

Before an experiment began, the sample was measured, and the mass was recorded. The linear-slide assembly was zeroed at the bottom of the crucible before the sample was then added into the

crucible. Measurements of the crucible's mass before and after the experiment were also performed in case any of the sample became stuck within the crucible.

During each measurement, both for calibration measurements and for the measurements of the salts themselves, the sample was heated to slightly above the maximum temperature in the desired range. At that high temperature, a quenching rod was used to stir the sample. This is to remove any bubbles that formed along the sides of the crucible. Once this was done, the temperature was reduced to the highest in the temperature range of interest. At each temperature step, the sample was allowed to reach an equilibrium in its temperature through it sitting at the temperature for a minimum of 30 minutes. Once that time had passed, three to four measurements were taken in which the electrodes were slowly lowered using the linear-slide assembly until the potentiostat read that the surface of the salt had been reached. After all measurements were taken, the sample was poured onto a section of Nickle foil which quenched it and allowed for it to be weighed.

When making calculations later, any significant outliers were thrown out and the average was taken of the height measurements. That average is the value that was then used to calculate the volume of the salt. Furthermore, the mass of the salt before and after was averaged and that average value is what was used to calculate the density.

3.3 BeF_2-NaF

3.3.1 Materials

Although the BeF_2-NaF had originally been ordered from UCB to the specified composition of 57mol%NaF and 43mol% BeF2, the salt was proven to be the incorrect composition upon ICP-MS analysis. Analysis showed that it was instead ~47mol% BeF2 and ~53mol% NaF. As such, the salt required modification by adding more NaF or BeF2 accordingly.

After each addition of each type of salt, the composition was tested again. Unfortunately, with each modification, the composition was consistently off. This bizarre happenstance turned out to have occurred as a result of the furnace that was being used. These furnaces, which had been used for thermal purification, had become permeated by excess oxygen. This oxygen would then release into the chamber of the furnace as it was brought up to high temperatures. This would then result in oxides being formed within the salt which in turn caused issues with the composition of the salt.

To remove those contaminants, HF purification had to be performed. HF purification began by purging the system with argon for 12 hours. The salt was then melted as the argon purge continued for another 12 hours. Next, the argon gas purge was concluded, and the H_2/HF purge was started and ran for 10 hours. Finally, another argon purge was done for 12 hours. Upon the completion of this purification, the salt visibly had less contamination. Where before it was rife with black and grey flecks, now those black flecks were few and far between.

However, since the furnace situation had yet to be entirely resolved, when the salt was melted down again, a thin layer of oxides formed as a film on its surface. This film was simply removed using a spoon. When the composition was tested yet again, it was finally close to the proper values at 43.502mol%BeF2 and 56.364mol%NaF with a small 0.135mol% U contaminant.

To verify that the salt was at an acceptable level of contamination, impurity analysis was done using OH and CS analysis. The results of this analysis are in Table 5,

Table 5: OH and CS impurity analysis of the BeF_2-NaF (FNaBe) samples.

BeF_2-NaF Modified					
OH	O (ppm)	H (ppm)	CS	C (ppm)	S (ppm)
Sample 1	891.36	26.02	Sample 1	18.55	0
Sample 2	1143.27	23.21	Sample 2	62.92	0
Sample 3	1192.55	24.54	Sample 3	35.84	2.07
average	1075.77	24.59	average	39.10	0.69
stdev	161.5563	1.40	stdev	18.26	0.98

With the confirmation that the samples had acceptable levels of impurities, the experiments could proceed.

With each experiment that was performed, glassy carbon crucibles were used. The DSC used was that of the SDT-650, and the density system was mentioned prior as well as in [3].

3.3.2 Melting Point

The melting point measurement for BeF_2-NaF is precisely the same as for FLiNaK only with a different temperature range. Table 6 displays the necessary calibration information that was collected before the experiment.

Table 6: Calibration data for the purpose of the measurement of FNaBe's melting point.

Melting Point Calibration			
	Measured (C)	Expected (C)	Deviation
Zinc	419.751	419.38	0.088%
Silver	964.373	961.63	0.284%
Aluminum	661.884	660.17	0.259%

3.3.3 Heat Capacity

The heat capacity measurements performed for BeF_2-NaF were performed before the measurements for NaOH-KOH. As such, the procedure is far less effective and far less polished. Instead of sapphire being used for both internal and external calibration, NaF was used for the external calibrations. The same calibration constant made with one measurement of NaF was applied to all three of the BeF_2-NaF heat capacity curves. In Figure 6, that NaF external calibration measurement is compared to a verification measurement of NaF and to the NIST NaF data.

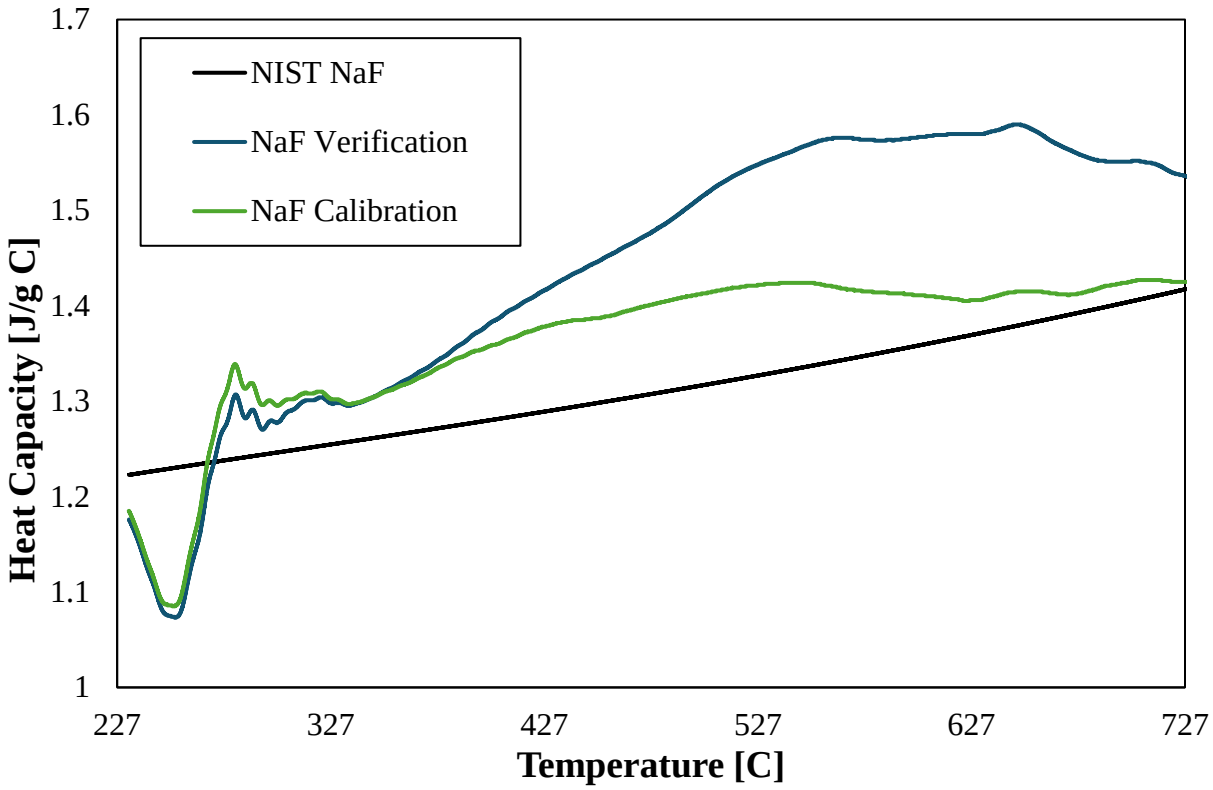

Figure 6: NaF calibration and verification curves for use in the measurement of FNaBe's heat capacity.

The calibration measurement of NaF and the verification measurement are quite close, implying repeatability and thus reliability of the measurement. This was no easy feat as multiple NaF calibration measurements had been conducted prior with little repeatability making them unusable. To demonstrate the reliability of the calibration constant formed from the NaF calibration curve in Figure 6, the calibration constant was applied to both the NaF verification data and sapphire verification data. These new curves are presented in Figure 7,

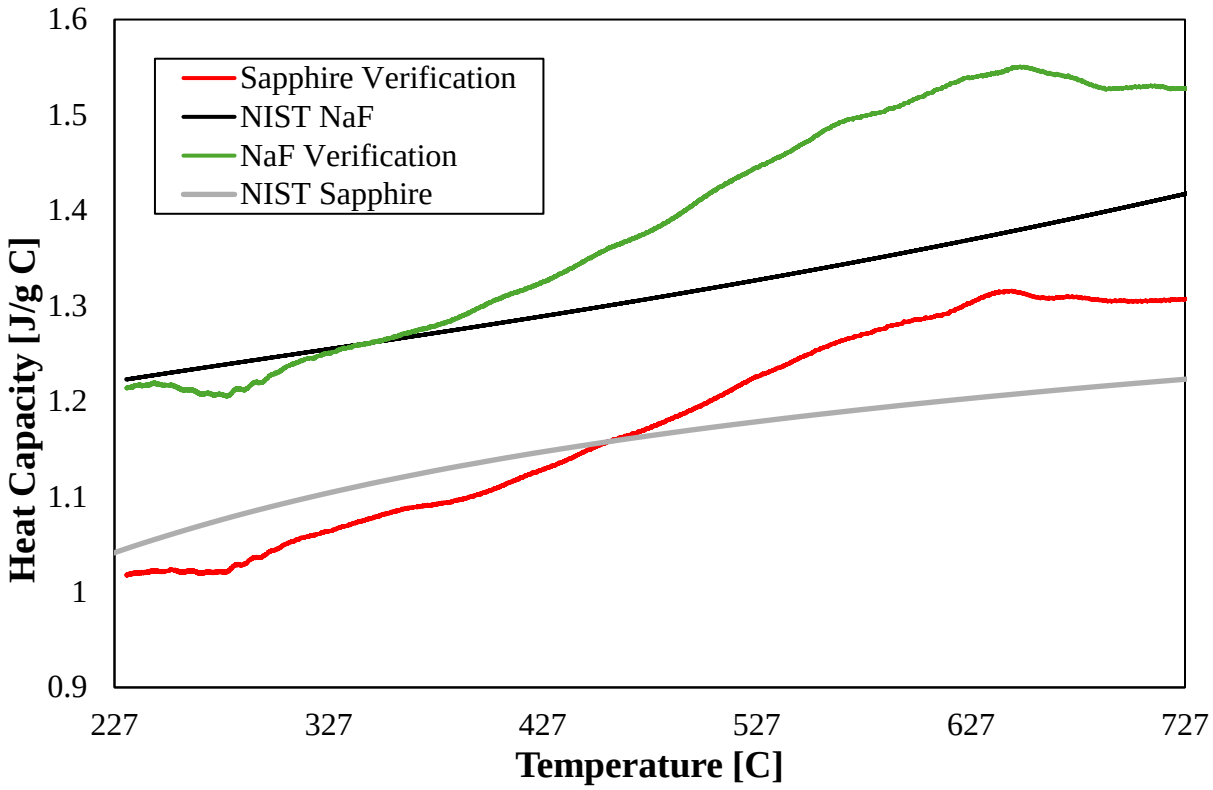

Figure 7: Verification data of NaF and Sapphire for the heat capacity measurements of FNaBe.

Additional differences between the NaOH-KOH procedure and this one is that the cleaning process was far less stringent. Yes, the crucibles were cleaned between each run, but the beams were not given as much attention. This is because BeF_2-NaF has far less of a corrosive effect on the beams in comparison to NaOH-KOH.

3.3.4 Vapor Pressure

The procedure for measuring the vapor pressure of BeF_2-NaF is the same as it is for FLiNaK. This includes the use of LiF for calibration. Only, the temperature range was that of 850C to 1010C instead of the prior values.

The LiF calibration curve is as follows in Figure 8,

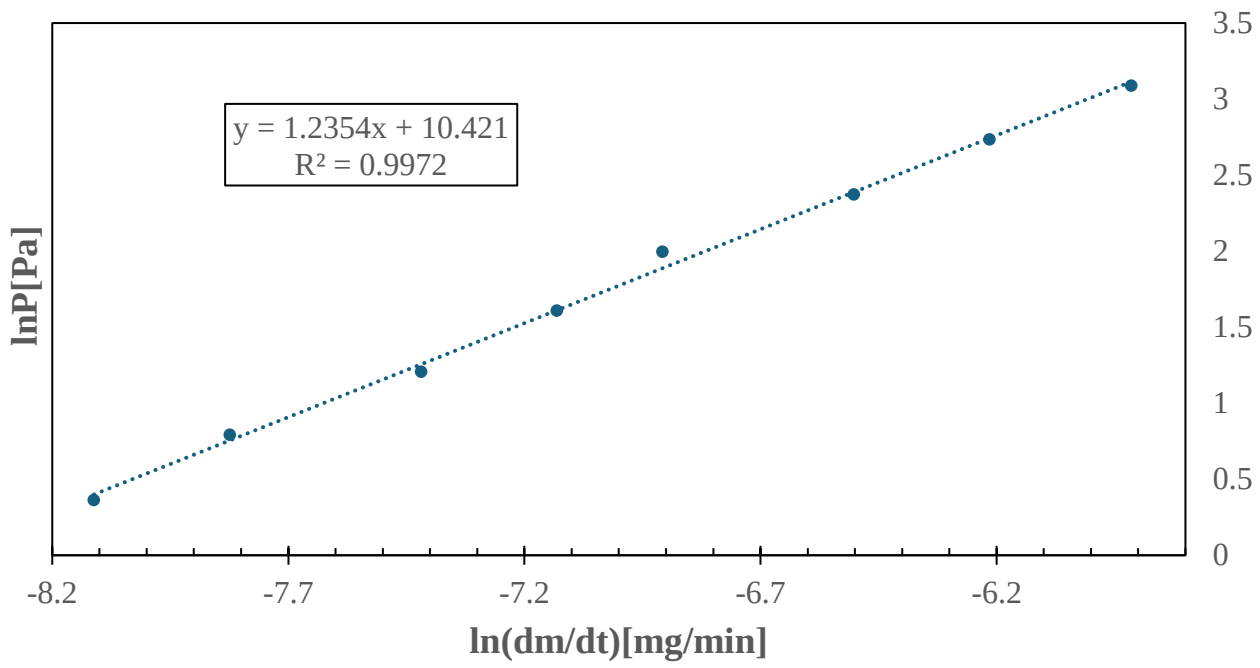

Figure 8: LiF calibration curve used for the vapor pressure measurements of FNaBe samples.

3.3.5 Density

The volume-height calibrations that were created using FLiNaK and were taken from [3] are as follows in Table 7,

Table 7: FLiNaK volume-height calibration curve equations which are used for the density measurements of FNaBe.

FLiNaK Volume-Height Calibration	
Temperature (C)	Volume-Height Curve
565	$V=0.08*h+1\times10^{-2}$
600	$V=0.08*h+7\times10^{-3}$
650	$V=0.079*h+2.1\times10^{-2}$
704	$V=0.079*h+3.3\times10^{-2}$
750	$V=0.079*h+1.5\times10^{-2}$
800	$V=0.08h-5.8\times10^{-2}$

The same procedure that was used for NaOH-KOH is used here for BeF_2-NaF.

Chapter 4

Results

4.1 FLiNaK

4.1.1 Melting Point

The expected value of the melting point of FLiNaK is 454C [1,2,3,45]. Upon conducting our own DSC analysis of the value, the melting point came out to be 451.7C. This value is within 0.5% of the expected value, and so our system can be said to be quite accurate.

4.1.2 Vapor Pressure

The FLiNaK vapor pressure data is displayed in Figure 9,

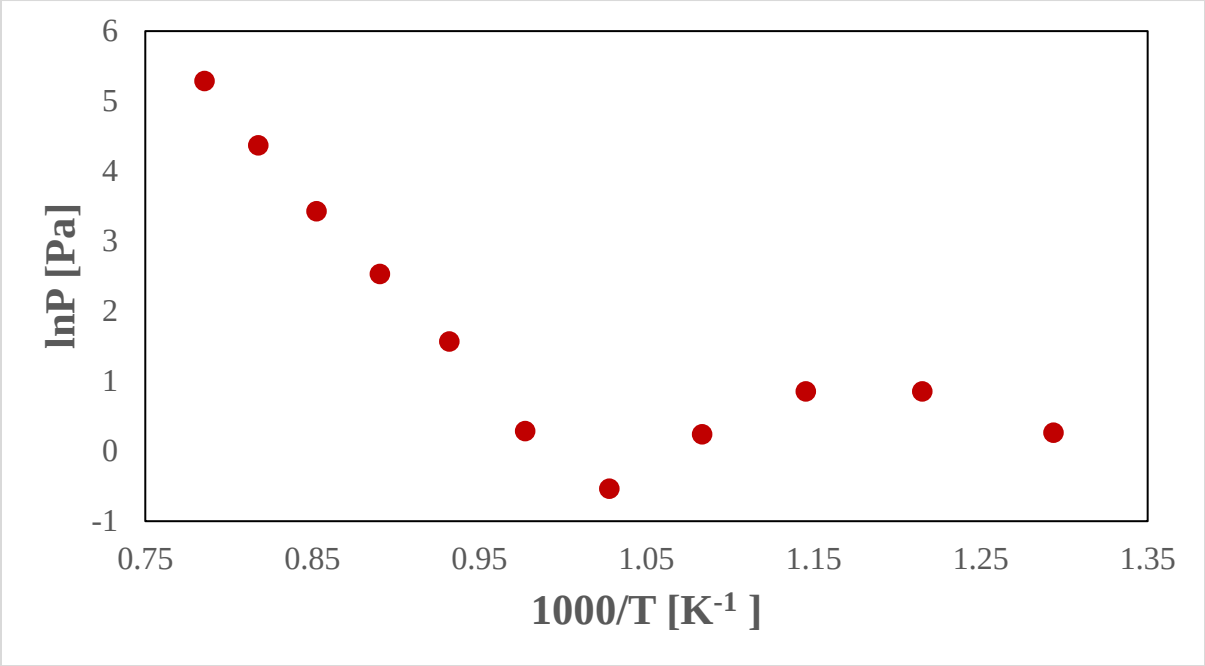

Figure 9: Vapor pressure data of FLiNaK prior to linear extrapolation.

Notably, the vapor pressure deviates from linearity past a low enough vapor pressure value. This is due to the machine not being sensitive to those values. However, the linearity before that value is quite strong and so that linearity was extrapolated to the lower temperature/ lower vapor pressure values in Figure 10,

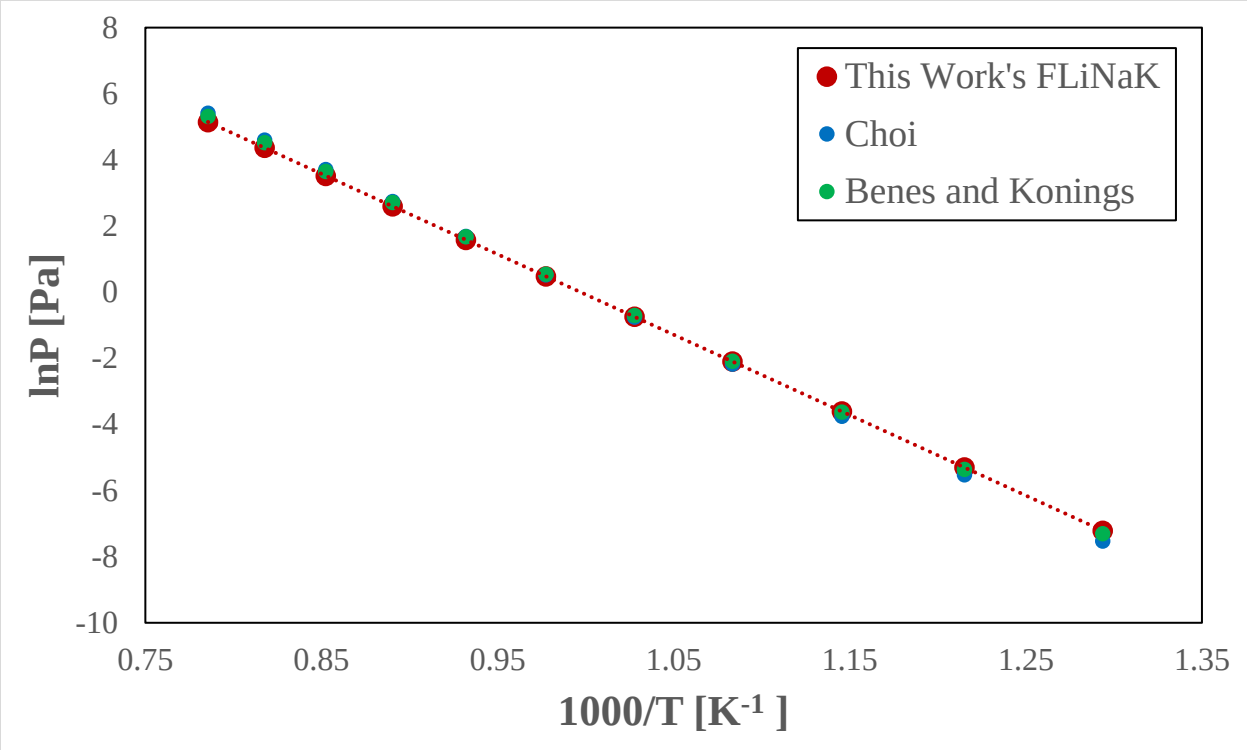

Figure 10: Linear extrapolated FLiNaK vapor pressure data with comparison to other works data, Choi [14] and Benes and Konings [45].

With the linear extrapolation, the vapor pressure was compared to other sources who had measured the vapor pressure of FLiNaK. As seen in Figure 10, the data of this study agrees quite well with the data of [14] and [45]. This verification leads to the conclusion that this method is indeed a reliable way to measure the vapor pressure of fluoride salts.

4.2 NaOH-KOH

4.2.1 Heat capacity

The first salt to be measured was salt sample 16 with composition 0.5NaOH-0.5KOH. As mentioned prior, the external calibration was initially performed using NaF salt and was then switched to sapphire. This switch occurred due to fluctuations observed in the NaF data that had been gathered to form the calibration constants as seen in Figure 11. In Figure 12 are the calibration constants after the

material was switched from NaF to sapphire. Additionally, for a clearer view of the data, Table 8 holds the calibration constants for NaF and sapphire across a range of temperatures.

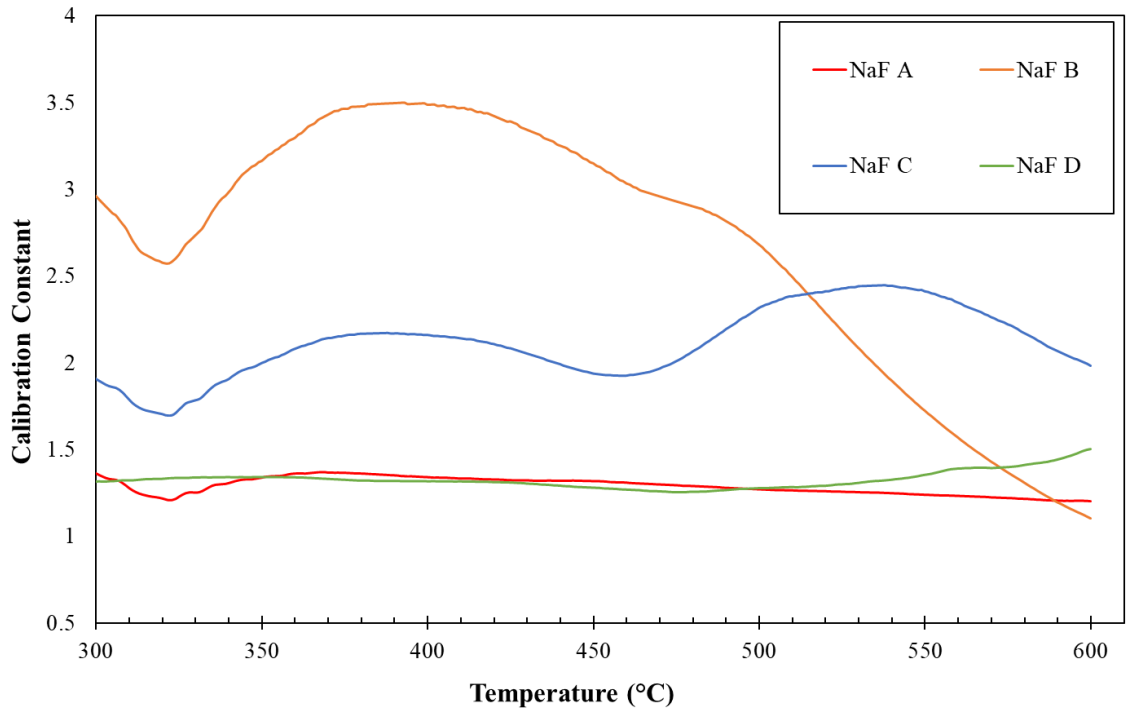

Figure 11: NaF calibration constants for salt sample 16.

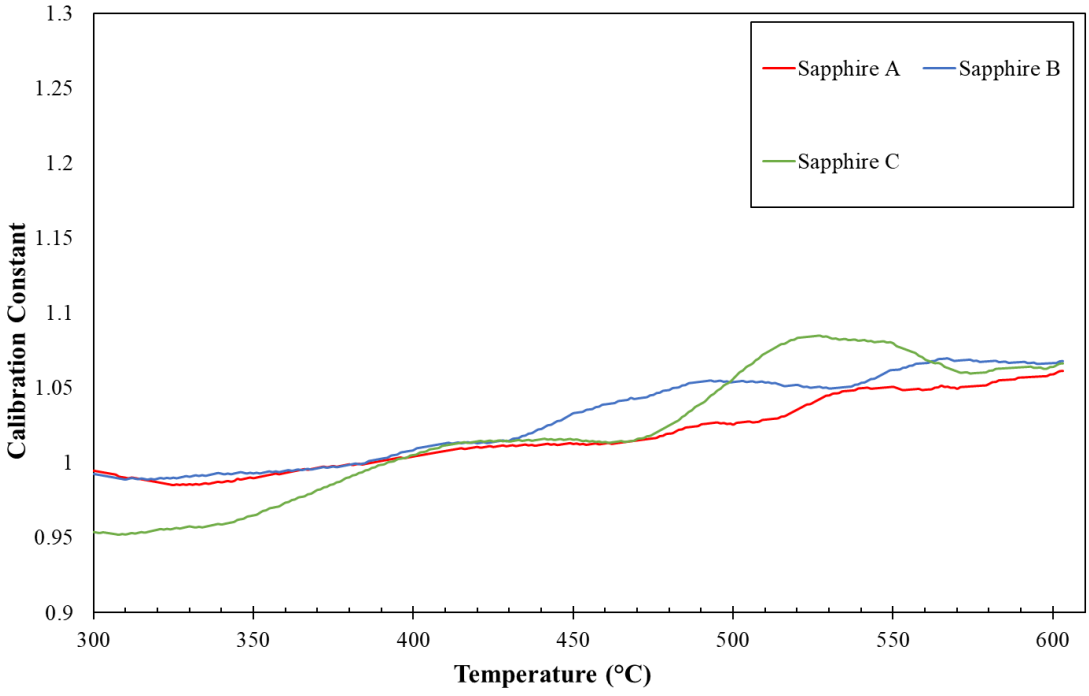

Figure 12: Sapphire calibration constants for salt sample 16.

Table 8: Calibration constants of sapphire and NaF over a range of temperatures.

	Sample Calibration Constants						
Temperature (C)	NaF A	NaF B	NaF C	NaF D	Sapphire 1	Sapphire 2	Sapphire 3
300	1.36	2.96	1.91	1.31	1.24	1.06	1.15
350	1.34	3.16	2.00	1.34	1.32	1.12	1.30
400	1.34	3.49	2.16	1.32	1.19	1.04	1.19
450	1.32	3.15	1.94	1.28	0.97	0.93	1.03
500	1.27	2.68	2.32	1.28	0.91	0.91	0.98
550	1.24	1.72	2.41	1.35	0.93	0.95	0.99
600	1.20	1.10	1.98	1.50	0.97	0.97	1.02

For an external calibration constant to be seen as usable, it should be around 1. The figures and Table 9 indicate that the calibration constants of NaF are far less consistent than for sapphire. The NaF calibration constants' curves all have different shapes, with only A and D being at all similar. Whereas the sapphire curves are all rather similar in both value and shape and are close to one. Therefore, sapphire external calibration is used.

Upon the collection of the calibration constants, the heat capacities were measured as seen in Figure 13 which displays heat capacity of salt sample 16 before external calibration is applied,

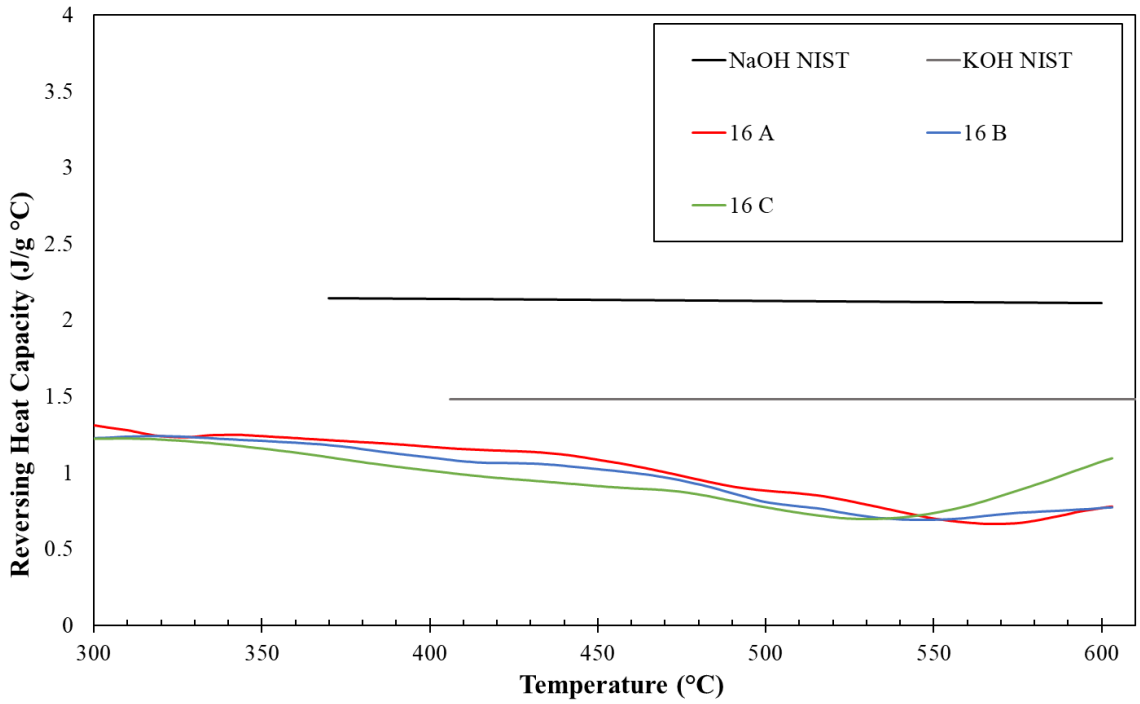

Figure 13: Heat capacity data for salt sample 16 prior to application of external calibration.

Once the data was gathered for each run, the external calibration was then applied via the multiplied calibration constant. This result is displayed in Figure 14,

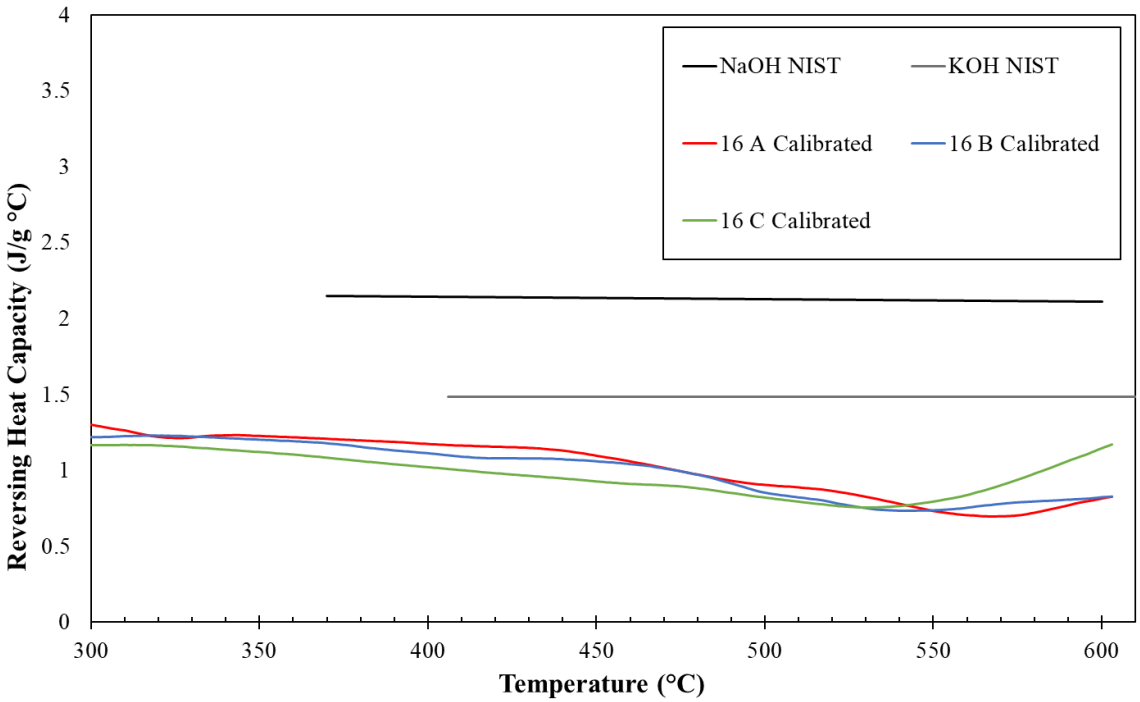

Figure 14: Heat capacity data for salt sample 16 with added external calibration.

As expected, considering the calibration curves of Figure 11, the NaF calibrated curves still show no similarity between one another, and the sapphire calibration curves are all very similar in both shape and value. It can comfortably be said that the datasets with sapphire external calibrations are reliable in comparison to the datasets with NaF external calibration, as such only sapphire was used going forward. Similarly, the changes to the cleaning procedures also resulted in more reliable data. However, considering the vaporization of the salt, using sapphire cannot take into account the effects of vapor on Cp measurements.

Once a reliable set of data was gathered, it was averaged and errors calculated as displayed in Figure 15,

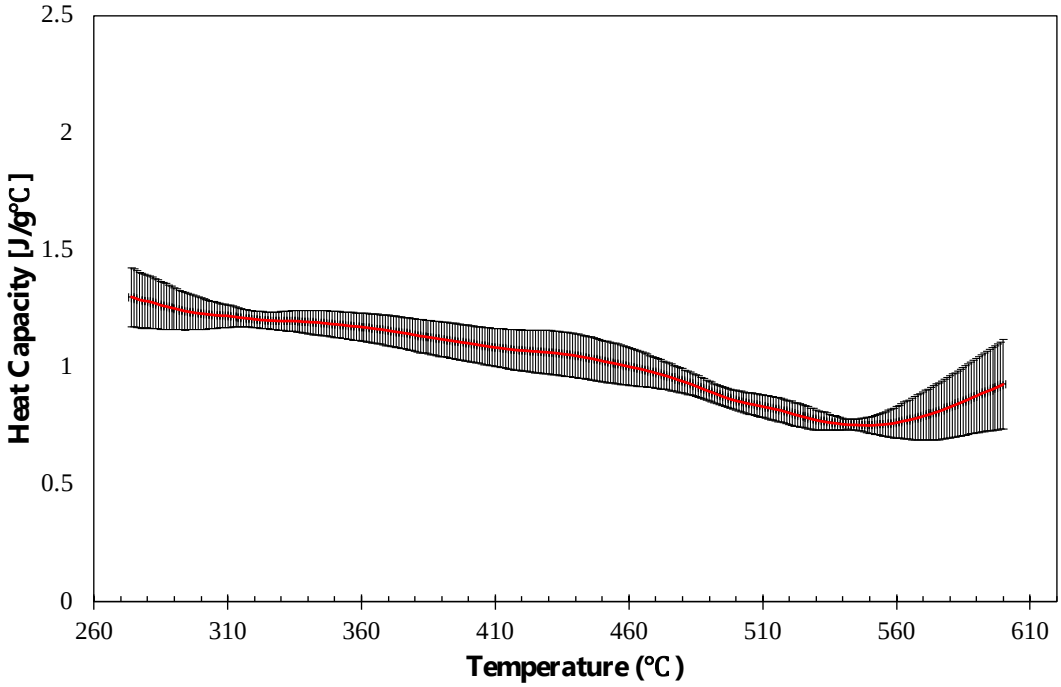

Figure 15: Averaged heat capacity data for salt sample 16 with calculated error.

The next set of data to be gathered was that of salt 17 with composition 0.55NaOH-0.45KOH. These datasets calibration curves are presented in Figure 16,

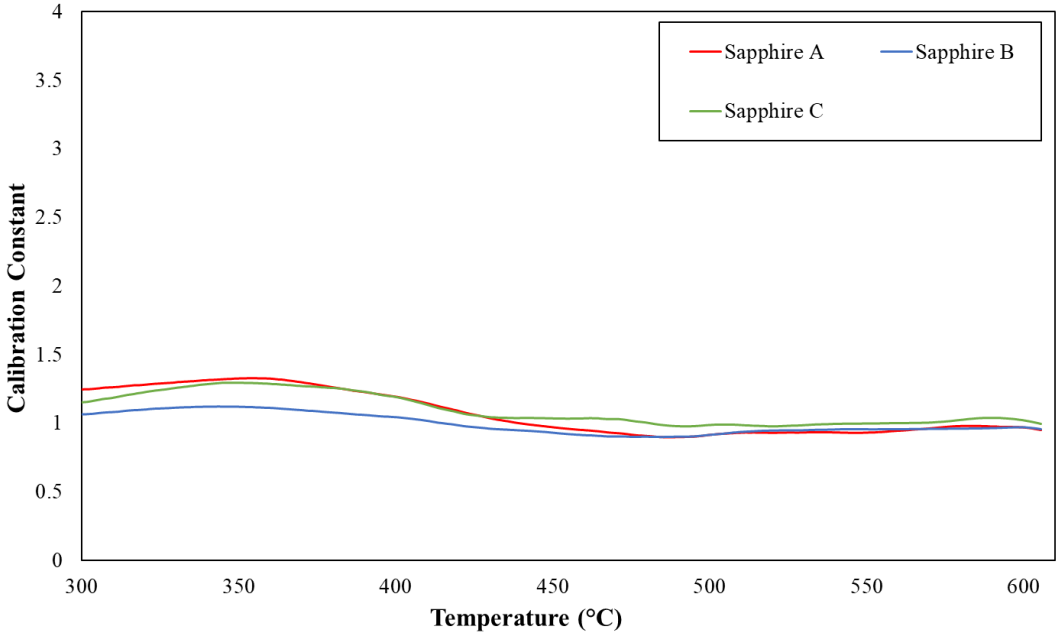

Figure 16: Calibration constants for salt sample 17.

As expected, the calibration constants are all similar in shape and sit close to 1, as such, collection of heat capacity data for salt 17 went forward. This data can be seen prior to the application of these calibration curves in Figure 17,

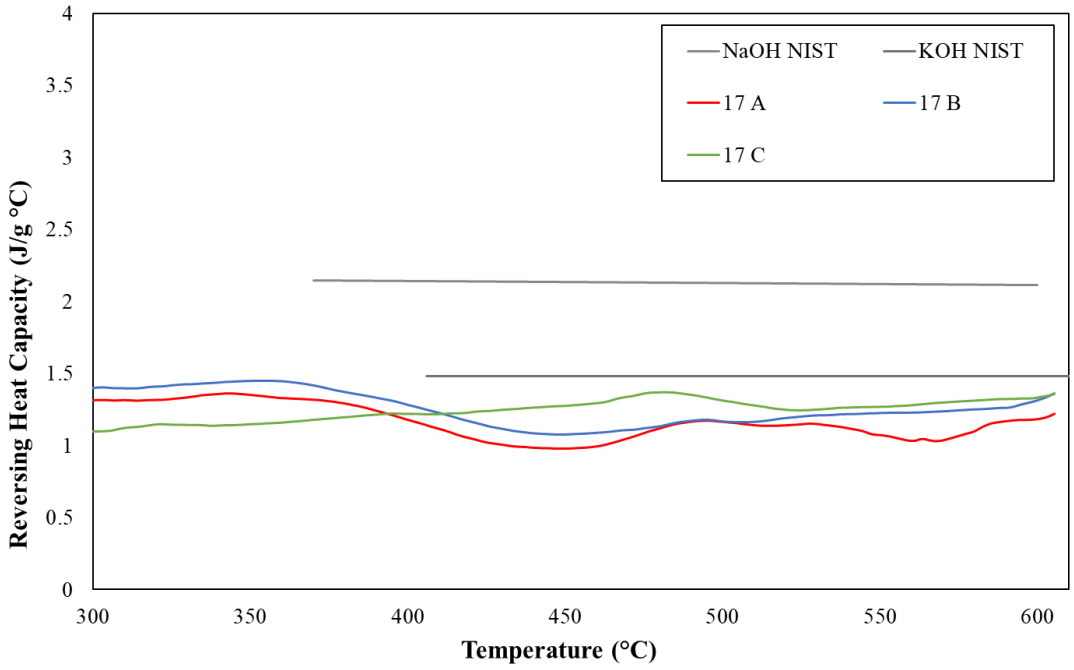

Figure 17: Heat capacity data for salt sample 17 prior to application of external calibration.

This dataset also is similar in shape and value. Next the calibration curves were applied to the data, displayed in Figure 18,

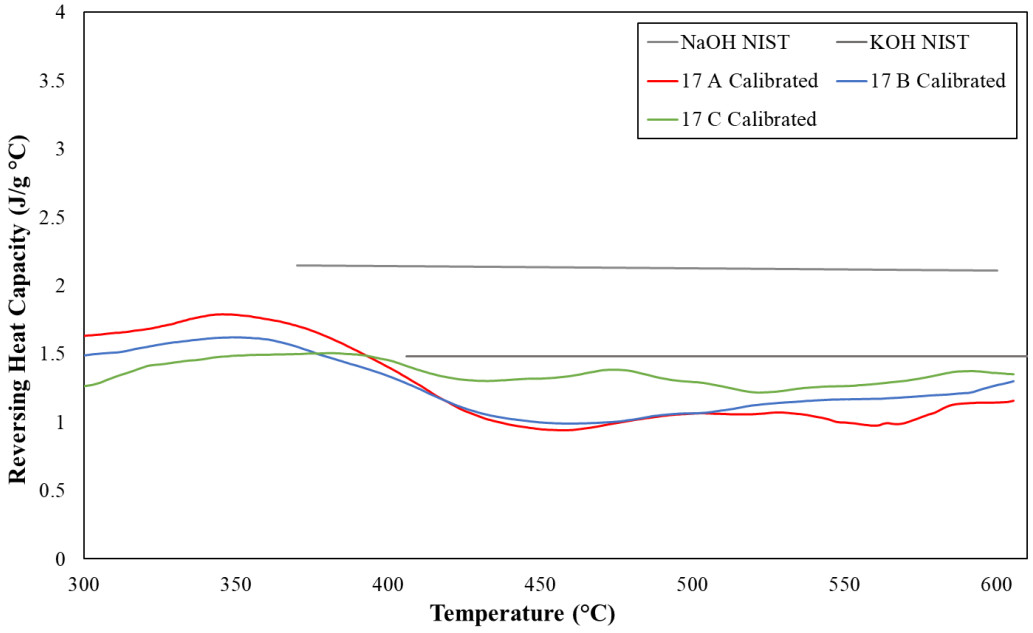

Figure 18: Heat capacity data for salt sample 17 with added external calibration.

As the data appears reliable in its similar shapes and values, the data was averaged and error calculated as seen in Figure 19,

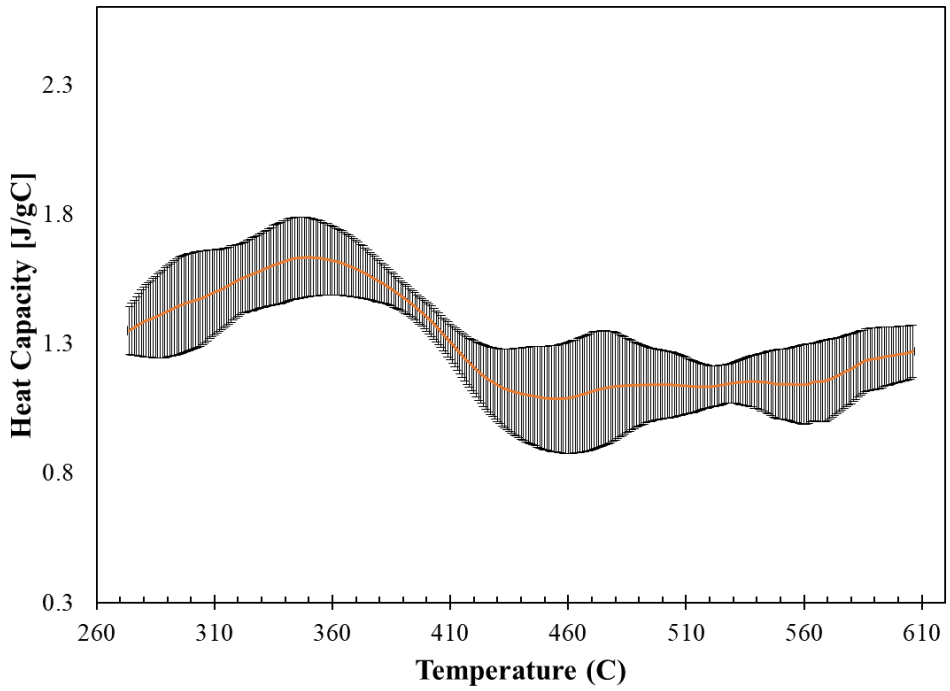

Figure 19: Averaged heat capacity data for salt sample 17 with calculated error.

Next salt sample 18 with composition 0.6NaOH-0.4KOH was measured. The calibration curves for this dataset are displayed in Figure 20,

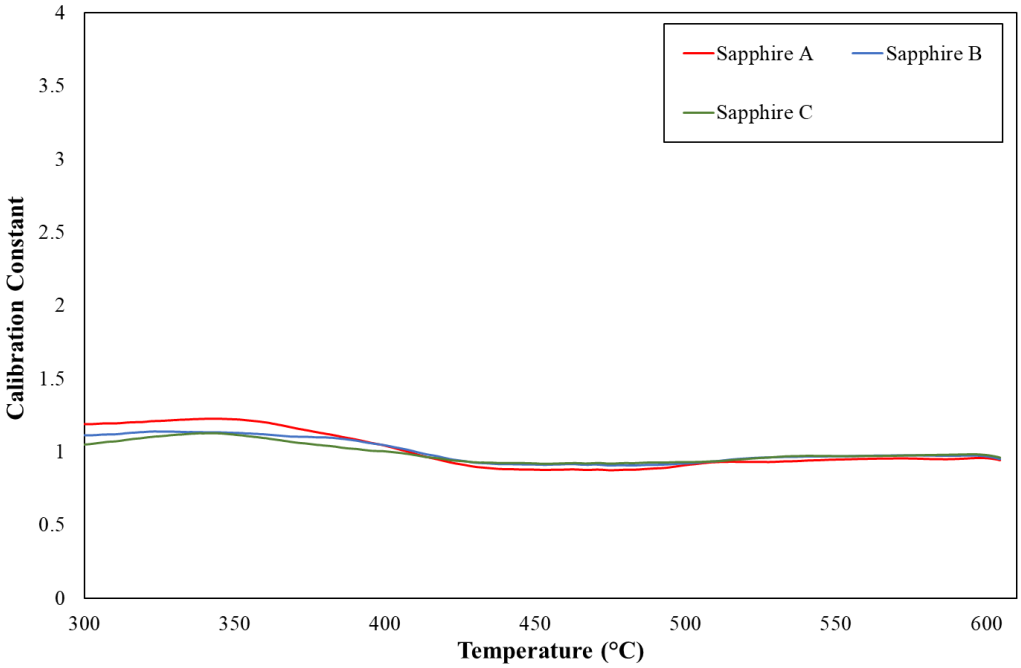

Figure 20: Calibration constants for salt sample 18.

With the calibration constants having a consistent shape and being close to 1, the heat capacity data for salt sample 18 was then gathered as presented in Figure 21 which does not have calibrations applied,

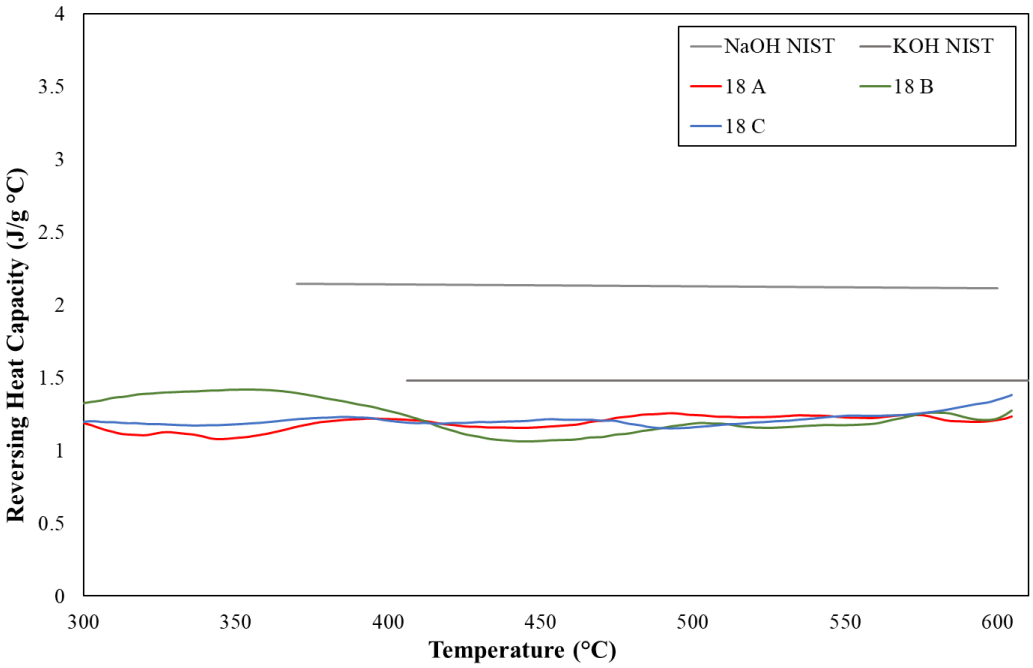

Figure 21: Heat capacity data for salt sample 18 prior to the application of external calibration.

The calibration constants as seen in Figure were then applied as seen in 22,

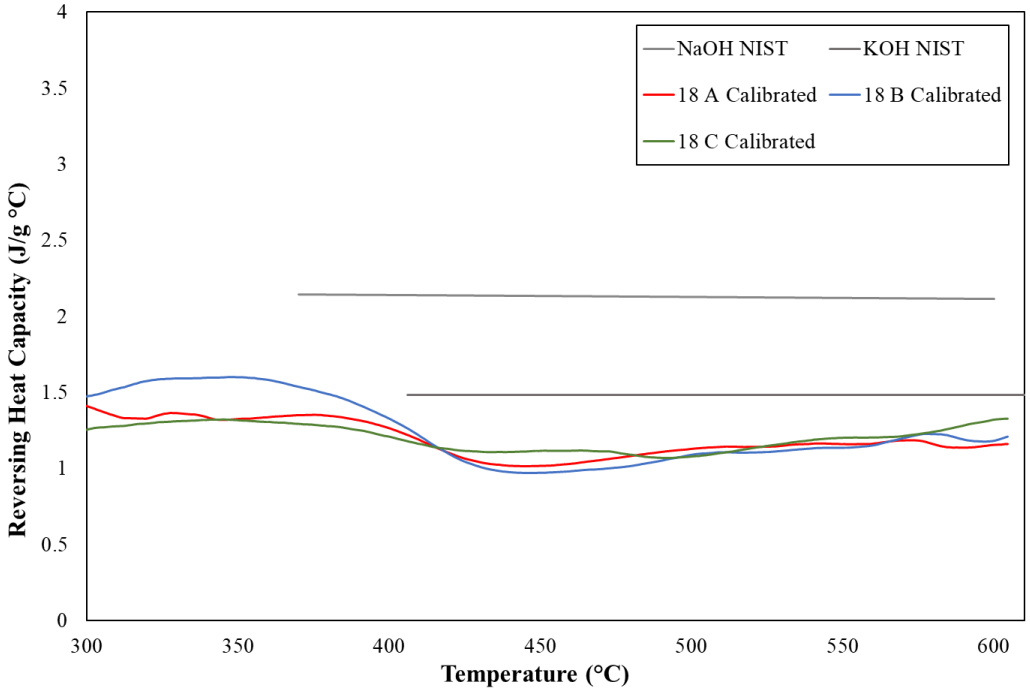

Figure 22: Heat capacity data for salt sample 18 with added external calibration.

Although dataset B seems to deviate slightly in the temperatures before 400C, the amount of deviation was not considered to be of too much concern and as such the data was kept and the average taken and the errors calculated as presented in 23,

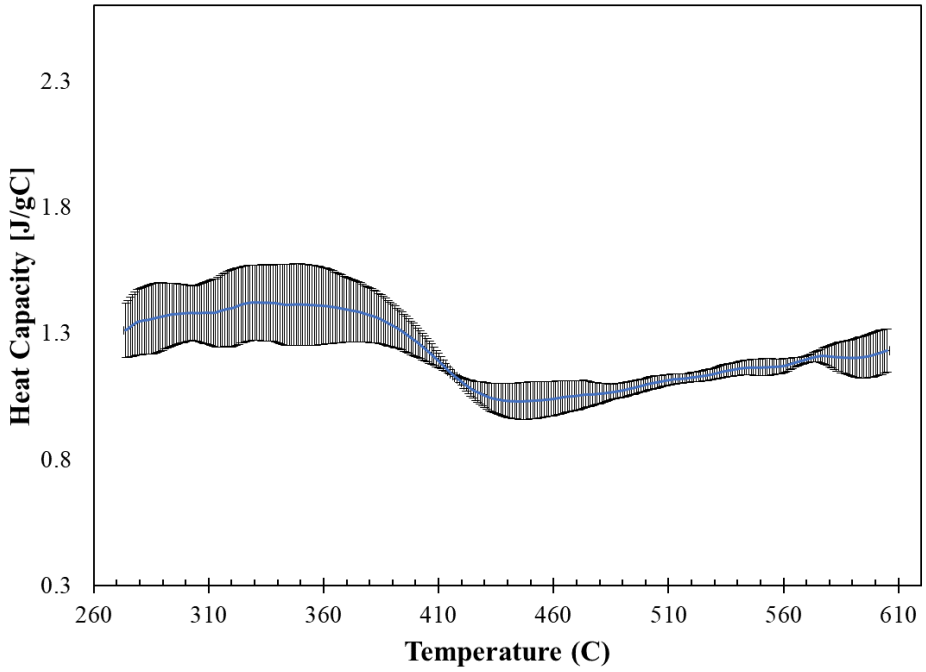

Figure 23: Averaged heat capacity data for salt sample 18 with calculated error.

As expected, the error prior to 400C is higher than the other sections of the graph, however, this error is not significant enough to be of concern.

After salt sample 18 was measured, the beams of the DSC broke and had to be replaced. After that replacement, the calibrations including temperature, heat flow, and mass all had to be re-done before measurements could proceed. New glassy carbon crucibles were also used due to previous ones having broken. Then, finally, salt sample 19 was measured. The calibration curves used are seen in 24,

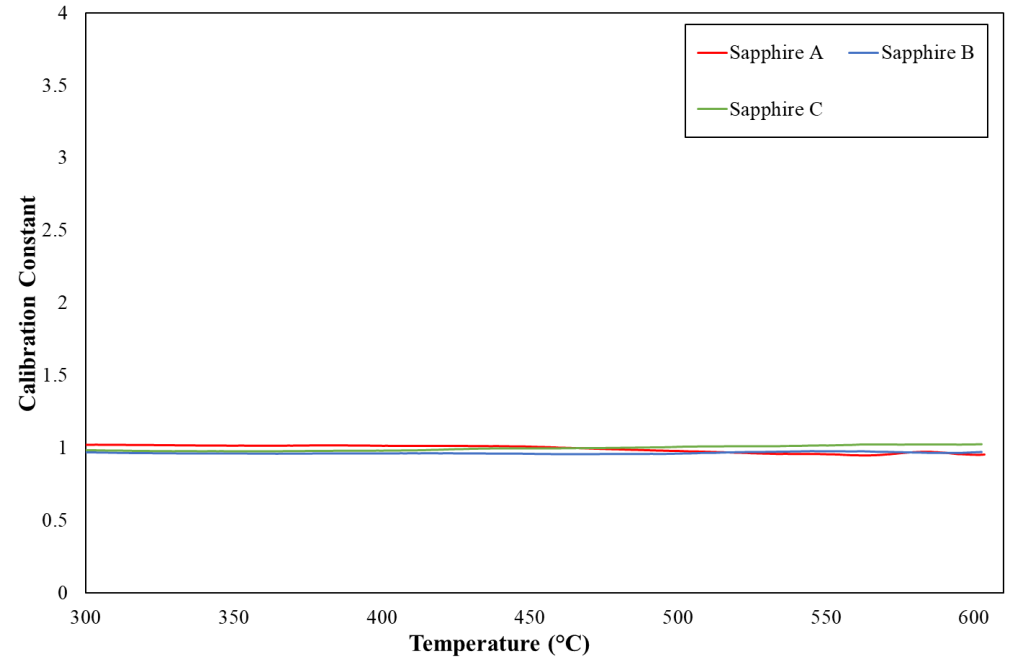

Figure 24: Calibration constants for salt sample 19.

With the Calibration constants being close to 1 and having an acceptable shape, the measurement of salt sample 19 proceeded as seen in 25 which does not include the added external calibration,

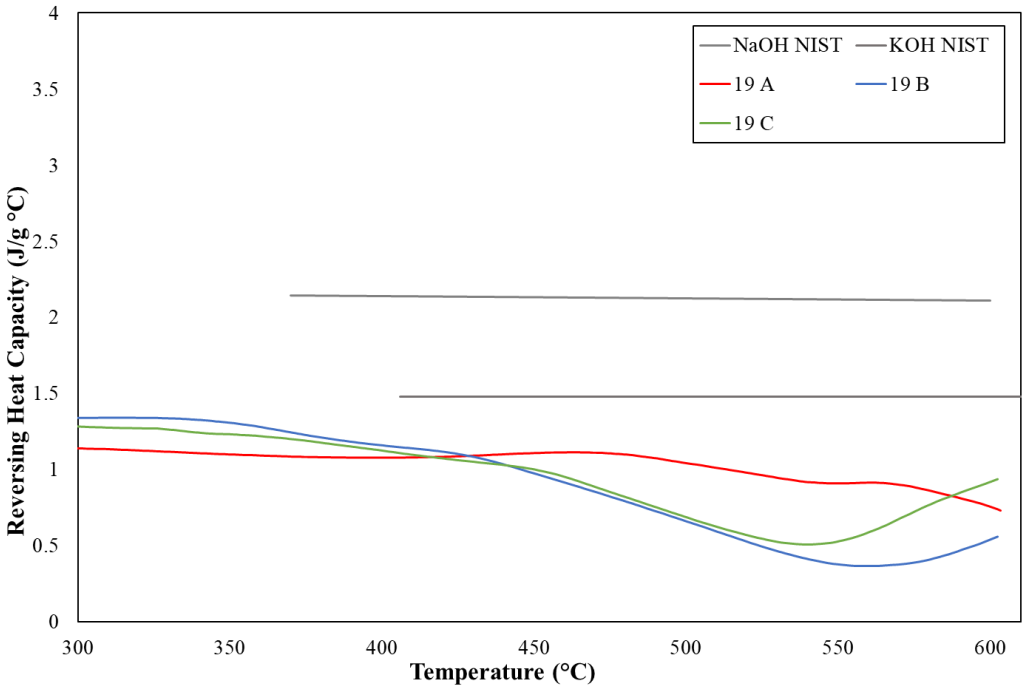

Figure 25: heat capacity data for salt sample 19 prior to the application of external calibration.

Although the curves display similarity in value and shape before 400C, after that temperature they do deviate slightly. Data in which the calibration curves were applied is displayed in Figure 26,

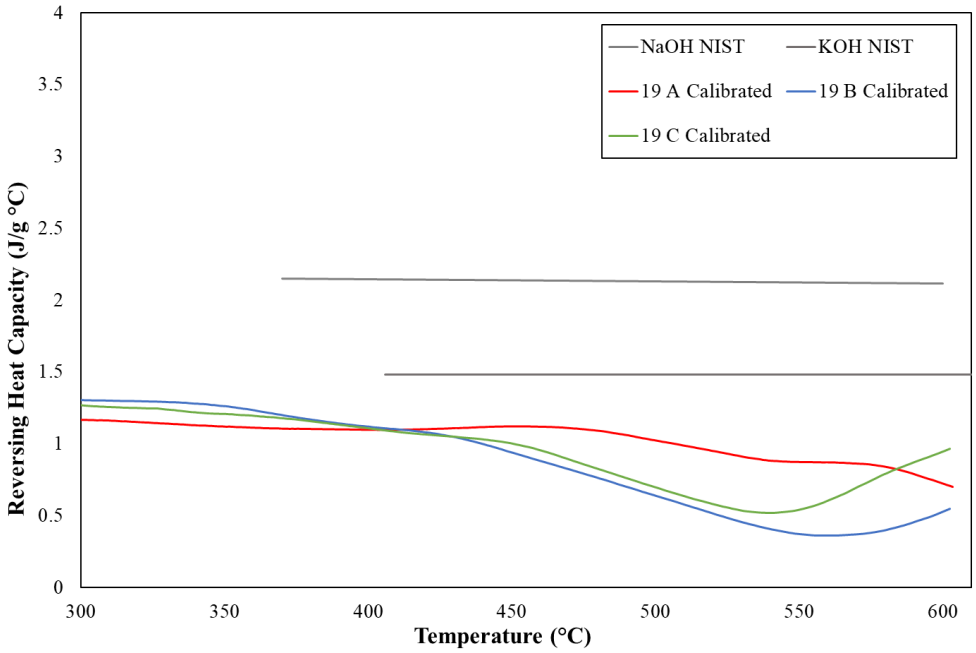

Figure 26: Heat capacity data for salt sample 19 with added external calibration.

Even after the application of the external calibration curves, the heat capacity after 400C is still observed to lack consistency in shape and number. Still, the curves were averaged, and the error calculated as seen in Figure 27,

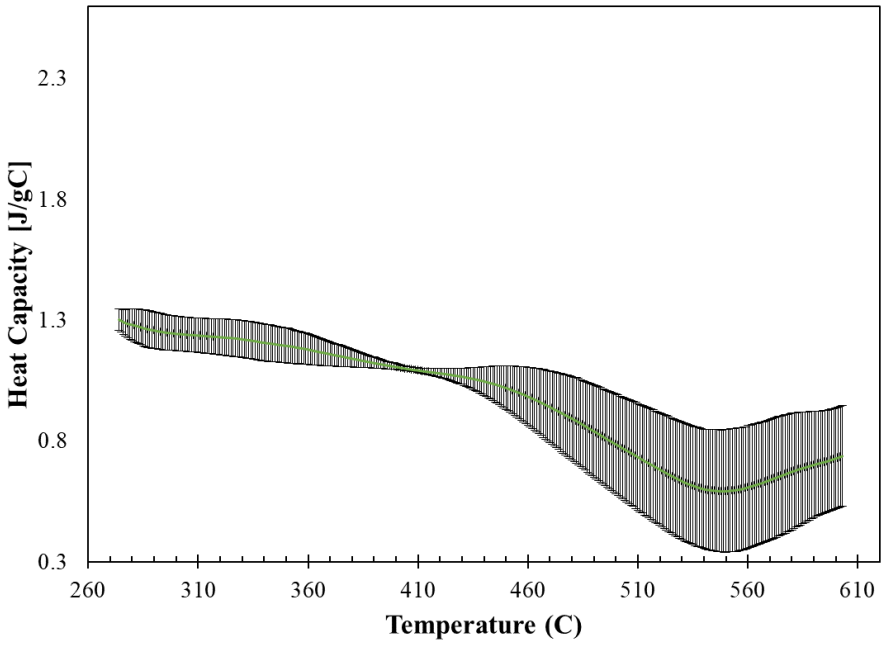

Figure 27: Averaged heat capacity data for salt sample 19 with calculated error.

As expected, the error is larger past 400C than it is before 400C. Still, this error is within acceptable values.

Next, the averages of the heat capacity for each composition were compared as seen in Figure 28 and Figure 29,

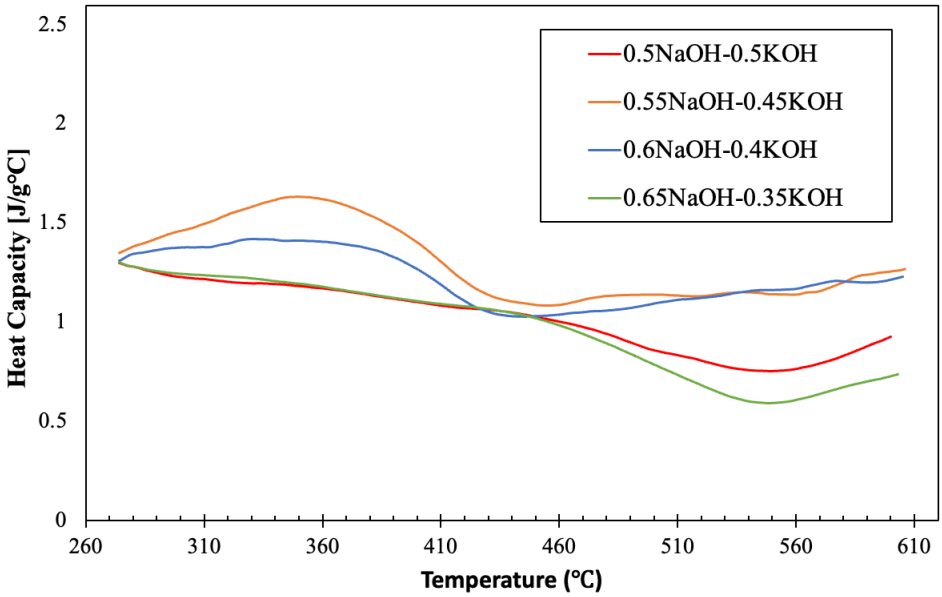

Figure 28: Averaged heat capacity data for all salt compositions in J/gC.

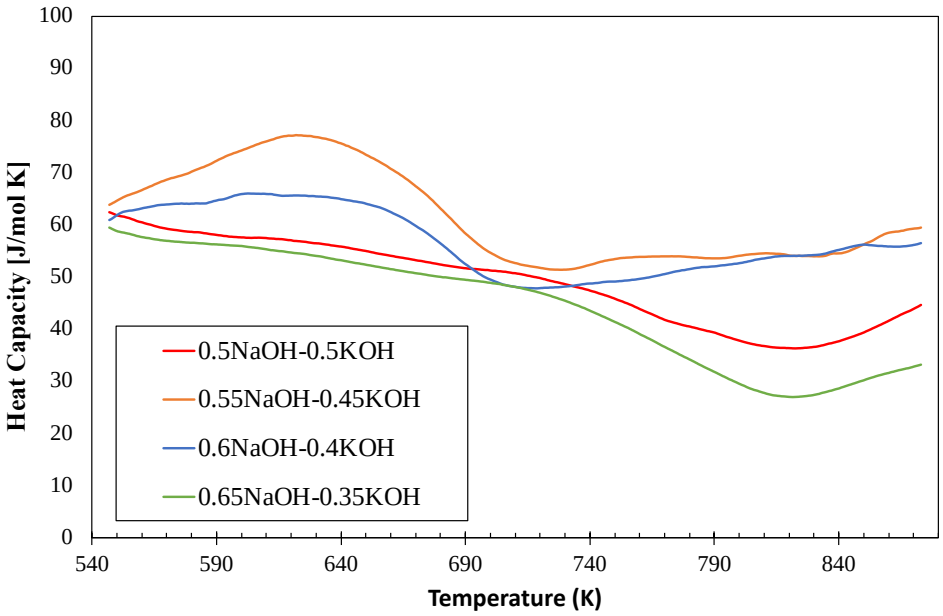

Figure 29: Averaged heat capacity data for all salt compositions in J/molK.

Notably, the averaged heat capacities of salt samples 17 and 18 have similar shapes with 17 having a slightly higher heat capacity than 18. The heat capacities of salt samples16 and 19 are also similar in shape and similar in value until around 430C where salt sample16's heat capacity is above salt sample 19's. However, salt sample 17's and salt sample 18's heat capacities are consistently above salt sample 16 and 19's heat capacities. This result is notably strange as with 16 sitting below 17 and 18 (and partially 19), this breaks the trend of the heat capacity becoming lower with higher mol%'s of NaOH. Also, it is noticeable that the two curves before the beams broke are similar (17 and 18), and the two curves after the beams broke are similar in shape (16 and 19). It is possible that, due to the difference in calibrations, the data took on a different shape. However, it is also possible that the corrosion of the beam affected the results of salts 17 and 18 since at the time of their measurement, the beam had already undergone multiple heat capacity measurements and some vapor pressure measurements of the hydroxide salt thus corroding the beam significantly. This possibility cannot be discounted despite the otherwise reliable appearance and repeatability of the results.

To summarize, all heat capacity data at relevant temperatures is displayed in Table 9,

Table 9: A summary of all heat capacity data both externally calibrated and not. Externally calibrated data is marked with a '.

	Sample Heat Capacities (J/g*C)																											
Temp. (C)	16 A	16 B	16 C	16 A'	16 B'	16 C'	16 Avg	17 A	17 B	17C	17 A'	17B'	17 C'	17 Avg	18 A	18 B	18C	18 A'	18 B'	18 C'	18 Avg	19 A	19 B	19C	19 A'	19 B'	19 C'	19 Avg
300	1.309	1.229	1.225	1.301	1.219	1.167	1.229	1.313	1.399	1.095	1.631	1.489	1.261	1.461	1.188	1.323	1.193	1.412	1.472	1.252	1.379	1.139	1.343	1.286	1.163	1.303	1.267	1.244
350	1.239	1.211	1.161	1.227	1.203	1.122	1.184	1.353	1.449	1.146	1.788	1.623	1.485	1.632	1.084	1.417	1.177	1.323	1.599	1.317	1.413	1.1	1.312	1.234	1.118	1.261	1.205	1.195
400	1.169	1.102	1.015	1.175	1.113	1.022	1.103	1.182	1.287	1.219	1.408	1.343	1.455	1.402	1.214	1.274	1.204	1.266	1.332	1.211	1.269	1.079	1.164	1.128	1.095	1.119	1.106	1.107
450	1.084	1.025	0.914	1.097	1.059	0.928	1.028	0.979	1.077	1.274	0.946	1.004	1.318	1.089	1.158	1.065	1.208	1.014	0.971	1.114	1.033	1.108	0.982	1.005	1.118	0.941	1.001	1.02
500	0.882	0.808	0.775	0.906	0.852	0.822	0.859	1.166	1.17	1.314	1.062	1.066	1.294	1.141	1.243	1.184	1.156	1.126	1.088	1.077	1.097	1.044	0.668	0.692	1.023	0.642	0.697	0.787
550	0.699	0.692	0.738	0.733	0.735	0.795	0.754	1.074	1.226	1.267	0.997	1.169	1.262	1.143	1.226	1.173	1.235	1.158	1.135	1.201	1.164	0.91	0.382	0.526	0.871	0.373	0.535	0.594
600	0.769	0.77	1.076	0.816	0.822	1.147	0.928	1.182	1.311	1.33	1.143	1.27	1.359	1.258	1.207	1.217	1.345	1.153	1.18	1.319	1.217	0.76	0.539	0.916	0.724	0.522	0.939	0.728

4.2.2 Density

The density of NaOH-KOH was gathered after the NaOH calibration curves were generated. The data gathered is presented in Figure 30,

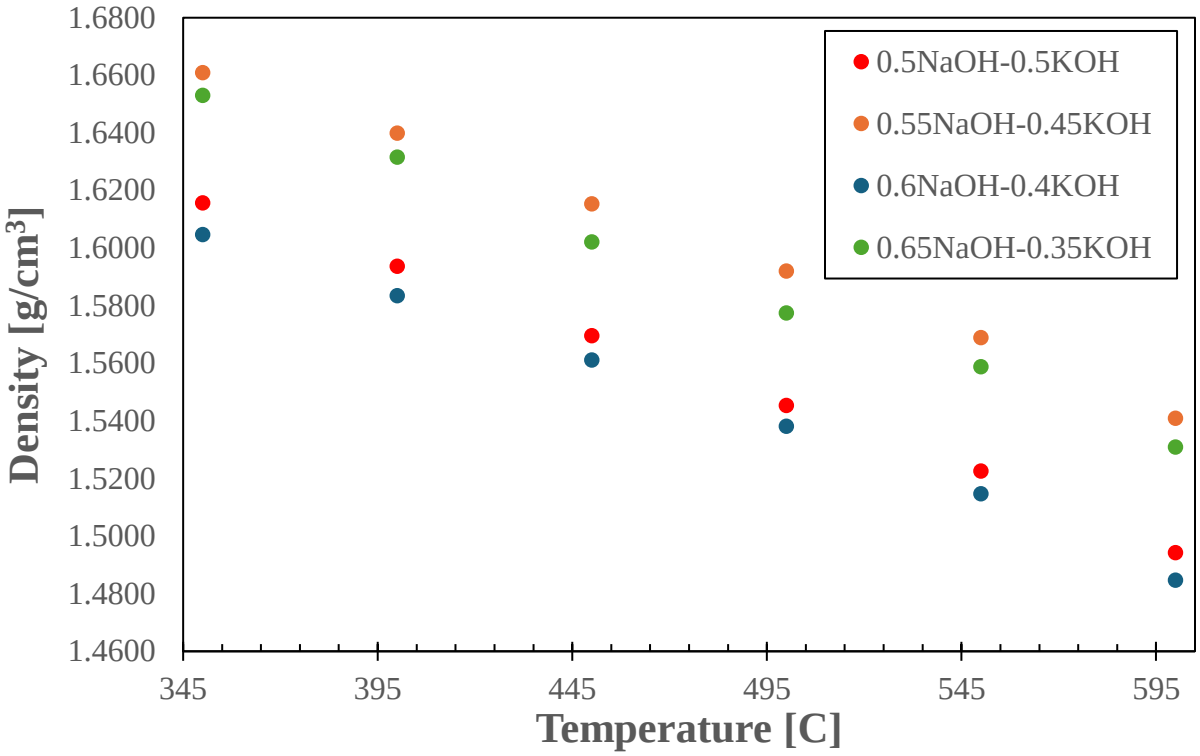

Figure 30: Density data of all four NaOH-KOH compositions.

Where the density temperature correlations of each salt composition are as follows in Table 10,

Table 10: Density-Temperature correlations of the four compositions of NaOH-KOH salt.

NaOH-KOH Salts	Density (g/cm^3) -Temperature (C) Correlation	Measurement Uncertainty [g/cm^3]
0.5NaOH-0.5KOH	$\rho = -4.827316 \times 10^{-4}T + 1.786188$	0.0287-0.0837
0.55NaOH-0.45KOH	$\rho = -4.776433 \times 10^{-4}T + 1.829920$	0.0201-0.0549
0.6NaOH-0.4KOH	$\rho = -4.738719 \times 10^{-4}T + 1.772921$	0.0364-0.0394
0.65NaOH-0.35KOH	$\rho = -4.877511 \times 10^{-4}T + 1.824040$	0.0246-0.0266

The density of each salt sample does not seem to be tied to the composition of the salt. This is not entirely unexpected. After all, the density of solid NaOH and solid KOH are quite similar at 2.12g/cm3 and 2.13g/cm3 respectively. Therefore, all the salt mixtures considered have close density values at the same temperature

4.3 BeF_2-NaF

4.3.1 Melting Point

Figure 31 displays the phase diagram for FNaBe as taken from the sponsors at the time (Thorcon). The curve displays a single expected phase transition for the composition of ~43.5% BeF_2 as labeled in green.

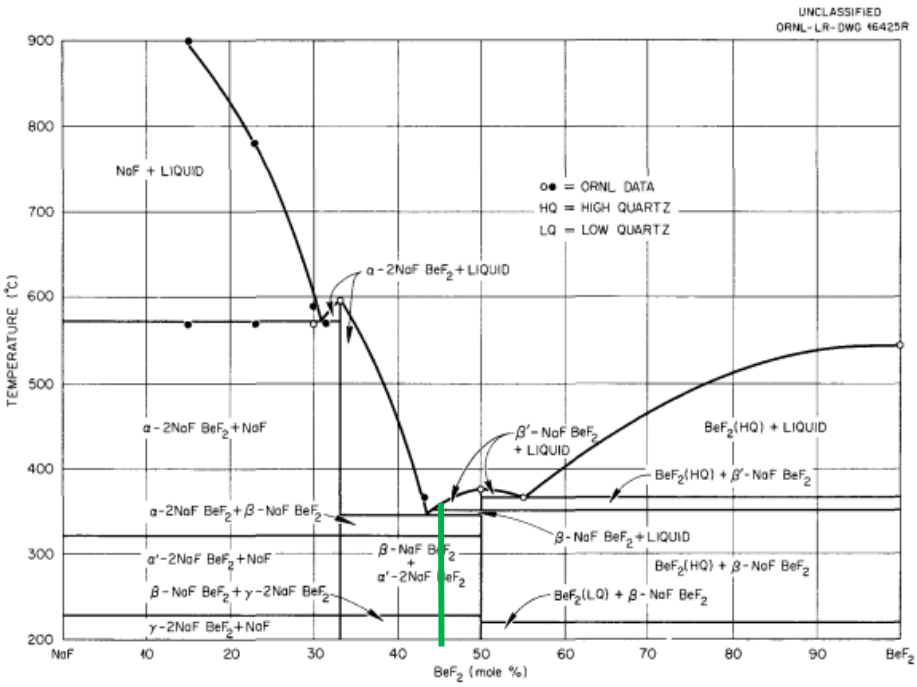

Fig. 3.20. The System NaF–BeF_2.

Figure 31: Phase diagram for FNaBe as provided by sponsors, Thorcon. *Green line indicates the composition of the modified salt.*

Upon examining the heat-flow curve obtained through the DSC, Figure 32, it appears that there are two peaks. Where the larger peak seems to start at around 340C, the second peak, which is partially within the first peak, appears to start at around 355C.

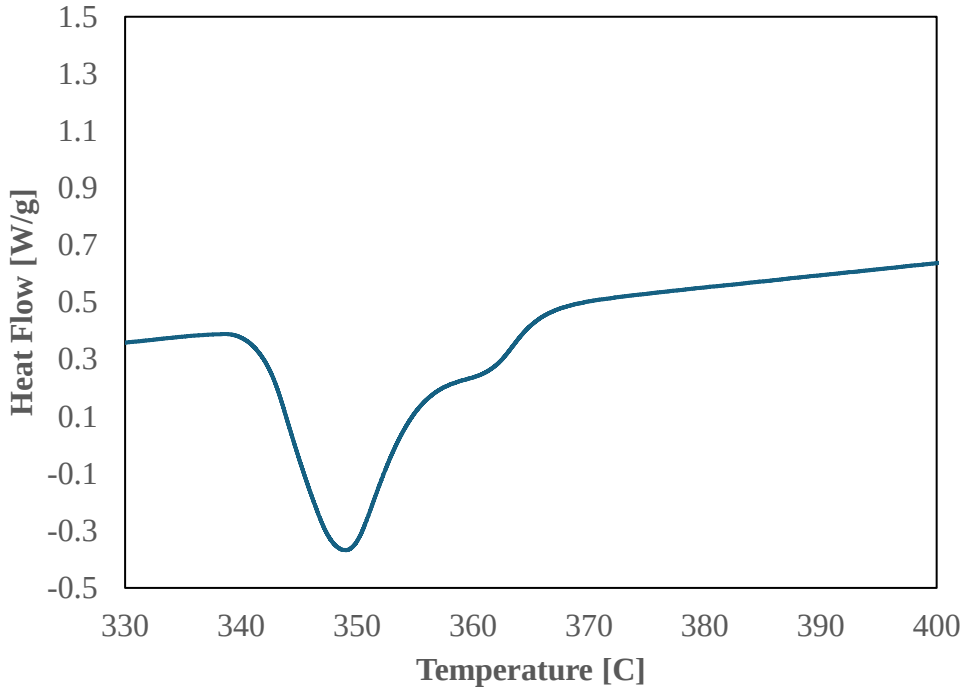

Figure 32: Heat-flow curve for modified FNaBe. Trial 2 at temperature increase rate of 3C/min.

Multiple measurements were taken of this salt. Each measurement displayed two peaks. The first peak represents the smaller pieces of the salt melding into each other as they melted, the eutectic point of the salt, but it is the second peak that represents the true melting point/ liquidus [46]. The results of using the DSC software to determine the temperature of that peak are in Table 11,

Table 11: List of heat-flow diagram parameters for the three trials of melting point measurements of FNaBe.

Peak Parameters	BeF_2-NaF Modified Trial 1	BeF_2-NaF Modified Trial 2	BeF_2-NaF Modified Trial 3
T_{ext} (C)	359.9	361.38	363.15

If so desired, it is possible to separate the two peaks for ease of determining the exact temperature of that second peak. That process is outlined in the discussion section and was not performed for the measurements of this study.

4.3.2 Heat Capacity

The heat capacity was measured a total of three times for the samples of FNaBe over the temperature of 473-1073K. According to the material properties and correlations report sent by the sponsors that these measurements were performed for, the expected heat capacity is around 2.18 J/gK. As seen in Figure 34 this report found the heat capacity to be closer to 1.35 J/gK. There are multiple reports that reference the 2.18 J/gK value, and upon further research it seems that that value comes from Cohen, et al. 1956 [32]. As mentioned in a prior section, the method with which they performed their measurements were rather archaic compared to the machines available today, such as the DSC. For this reason, it is not improbable that those results are not as reliable as the results given in this report.

All three trials of the heat capacity data are displayed in Figure 33,

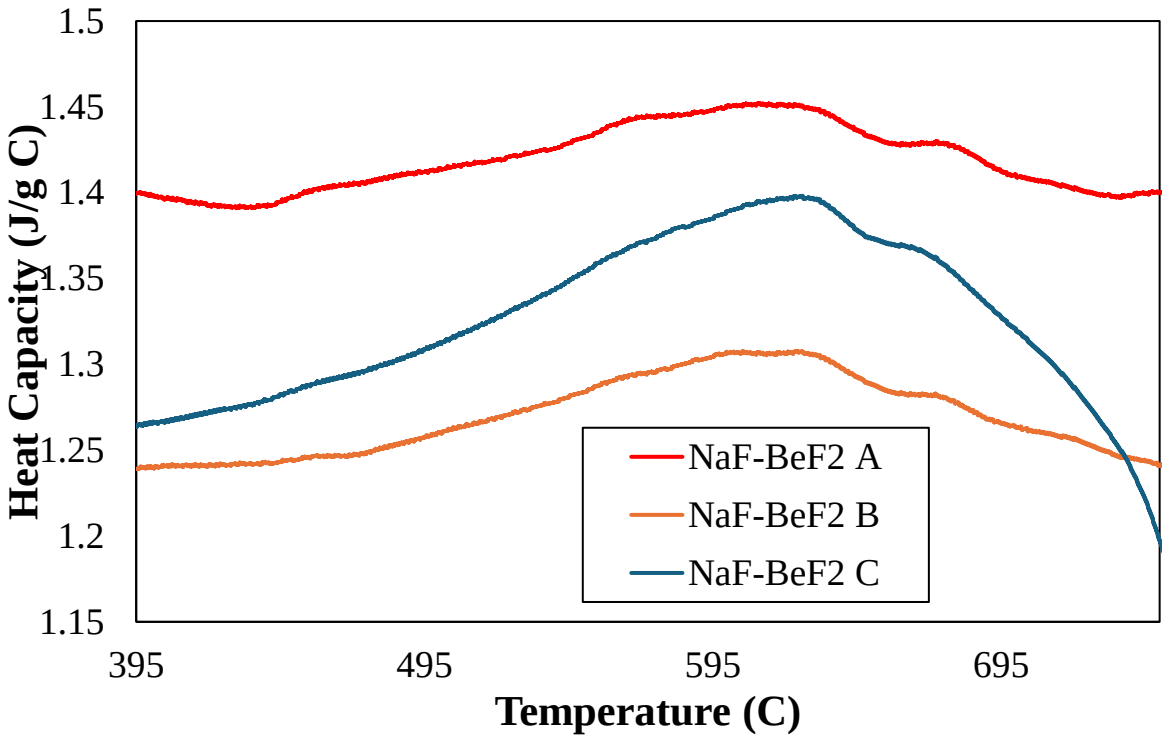

Figure 33: All three trials of measurements of the heat capacity of FNaBe found using DSC.

The average of the three trials is in Figure 34,

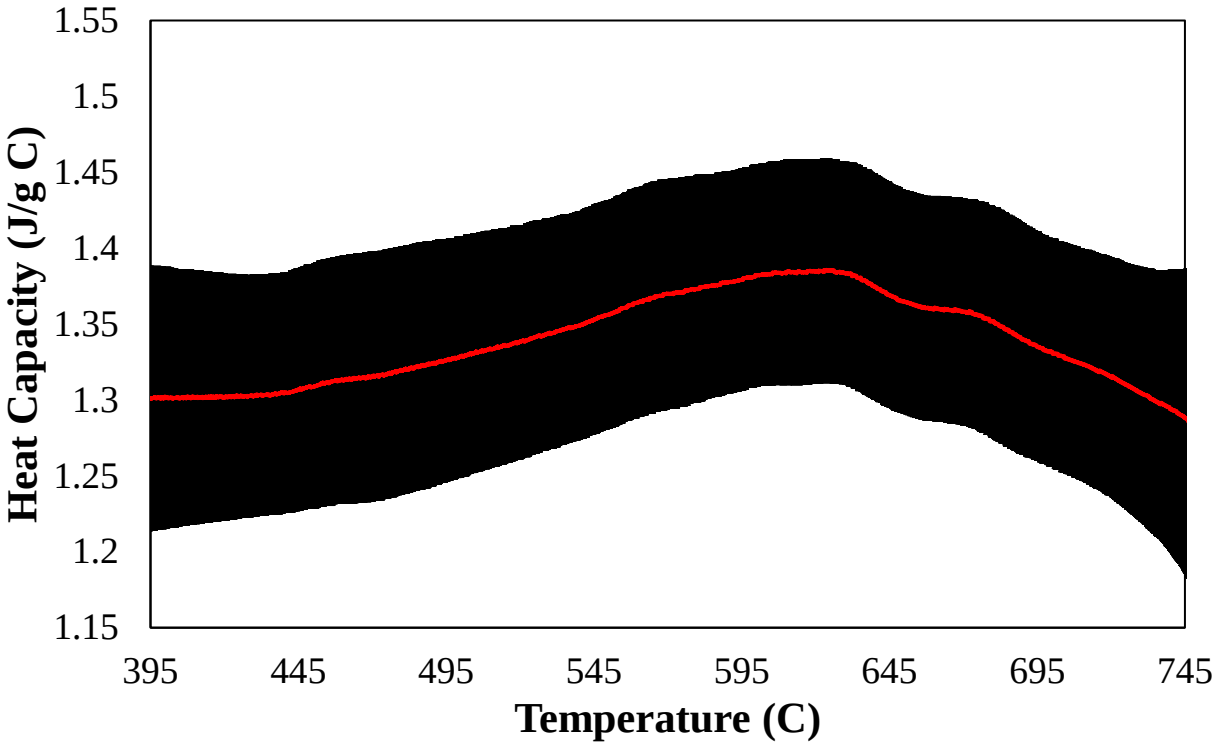

Figure 34: The averaged heat capacity of FNaBe.

Of important note is the fact that the curve consistently trends downwards at around 600C. While this could be the result of the NaF calibration being inferior to using sapphire as the calibration material, the curve itself does not vary enough for this to be of concern considering the highest it reaches is 1.39J/gC and the lowest is 1.29 J/gC. A variation of 0.1J/gC is acceptable.

4.3.3 Vapor Pressure

The vapor pressure of FNaBe, as averaged between the three measurements that were performed, is seen in Figure 35,

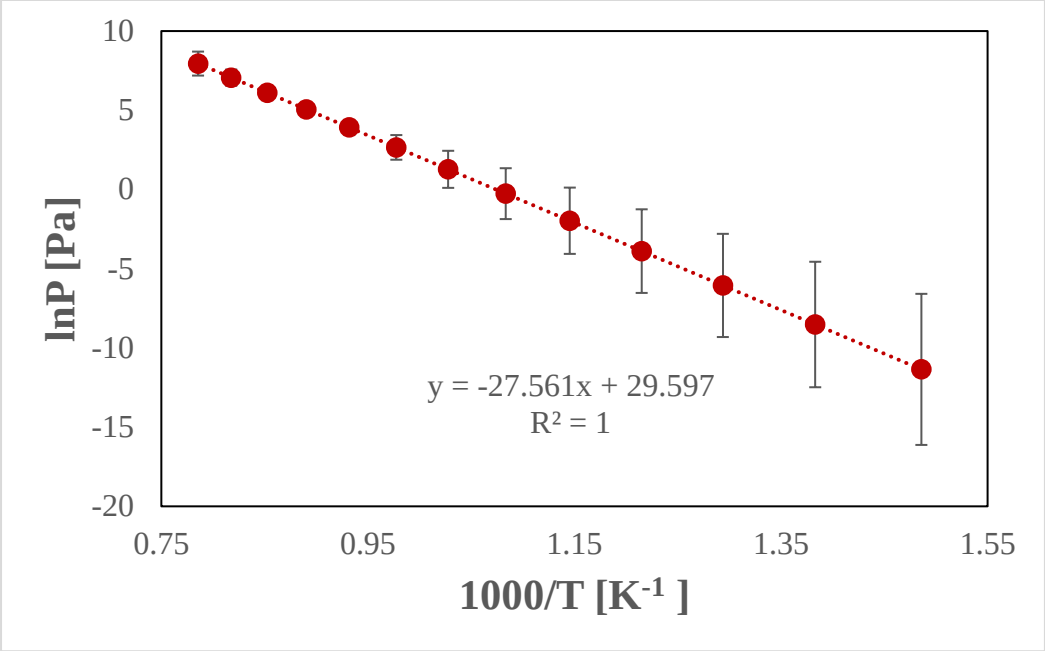

Figure 35: Linear extrapolated vapor pressure of FNaBe.

As the error bars indicate, the measurements at higher temperatures are more reliable than those of the lower temperatures. This is due to the DSC not actually being sensitive enough to measure vapor pressures that are so low, as is the case at lower temperatures. As a result of this lack of sensitivity, the raw data, Figure 36, shows a deviation from linearity,

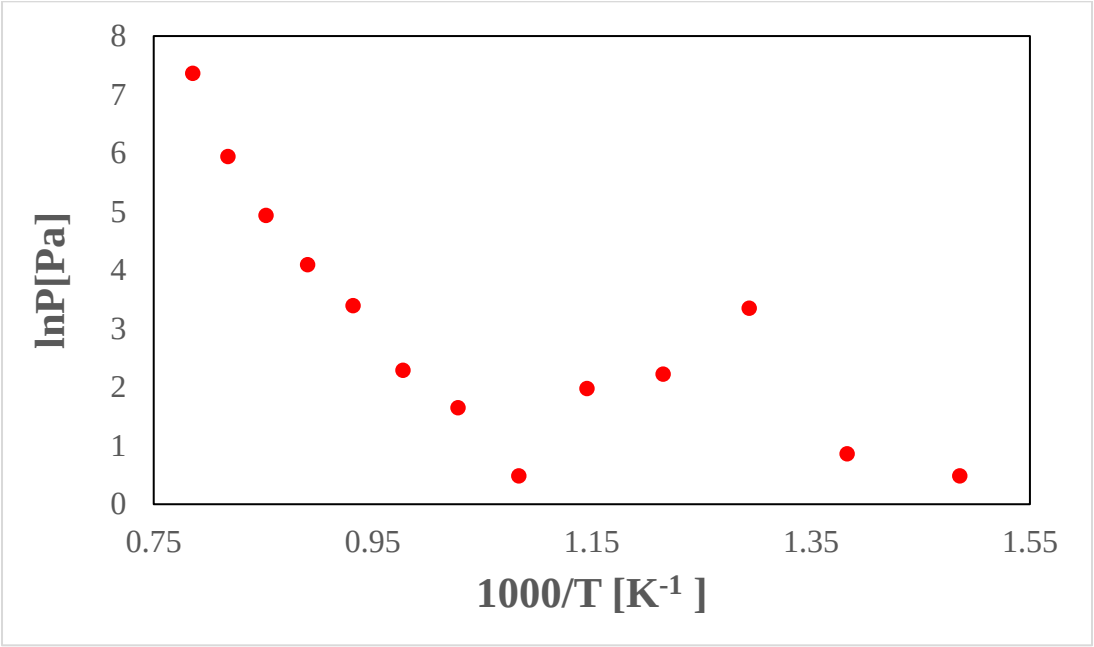

Figure 36: Vapor pressure data of one sample of FNaBe prior to linear extrapolation.

However, the data points prior to the sensitivity cutoff display such strong linearity, that that relationship was extrapolated to the lower temperatures as seen in Figure 35.

4.3.4 Density

Density measurements were collected over 565-800C for both the modified FNaBe and the FNaBe as received from UCB. The density-temperature correlations of those two salts are in Table 12,

Table 12: Density-temperature correlations for the two different compositions of FNaBe.

BeF_2-NaF	Density-Temperature Correlation	Measurement Uncertainty [g/cm^3]
Modified	$\rho = -3.776048 \times 10^{-4}T + 2.372570$	0.0175-0.0436
As-Received	$\rho = -3.555741 \times 10^{-4}T + 2.255968$	0.0153-0.016

In Figure 37, that data is plotted along with the ideal mixture values, UCB's data, and literature values from Cohen et al. [32].

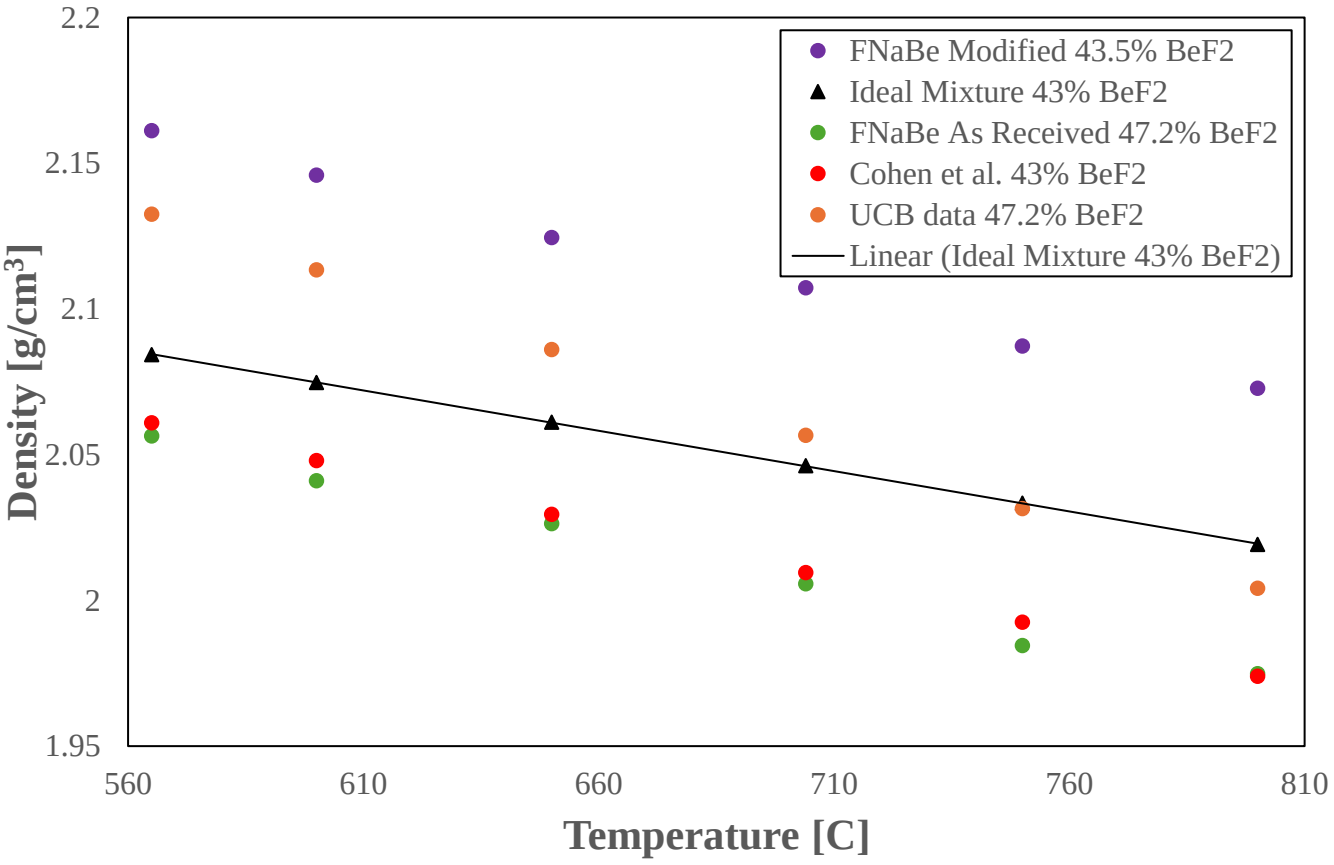

Figure 37: A comparison between the densities of FNaBe of differing compositions

Despite differing compositions, there is little trend to be seen in the data. BeF_2 has a density of 1.99g/cm^3 and NaF has a density of 2.56 g/cm^3, so one might expect that the FNaBe samples with more NaF would have a higher density. However, the literature value of the density which has 57% NaF sits very close to the as-received value of the density which has 52.8% NaF. However, because the data is all very close to one another, this lack of a trend is acceptable and points towards an overall density-temperature correlation of FNaBe that can be expected for most compositions at and close to the composition of 43% BeF2 57% NaF.

Table 13 displays the measured values of the density at each temperature and the ideal mixture value of the density at each temperature. There is a notable deviation from the ideal mixture values, especially for the modified salt.

Table 13: A comparison between the measured and ideal mixture values of the densities of FNaBe samples.

Temp., K	BeF_2-NaF Modified (43.5% BeF2)			BeF_2-NaF UCB (47.2 % BeF2)		
	Measured	Ideal Mixture	Deviation, %	Measured	Ideal Mixture	Deviation, %
565	2.1612	2.0843	3.56	2.0565	2.0741	0.85
600	2.1459	2.0748	3.31	2.0410	2.0654	1.18
650	2.1245	2.0611	2.98	2.0263	2.0528	1.29
704	2.1072	2.0462	2.89	2.0057	2.0391	1.63
750	2.0873	2.0334	2.58	1.9846	2.0272	2.10
800	2.0728	2.0192	2.73	1.9749	2.0142	1.95

Chapter 5

Discussion

5.1 Beam Change

As mentioned prior, after measurements were performed for NaOH-KOH salt sample 18, the beams broke and had to be replaced. Photos of the broken beams can be seen displayed in Figure 38,

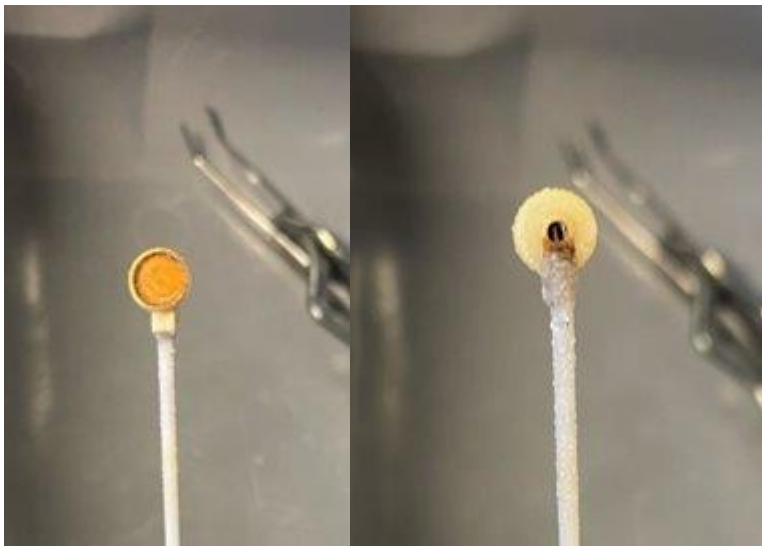

Figure 38: Alumina DSC beams corroded by hydroxide salt.

These beams are made of alumina which reacts with the hydroxide salts used in this report. With even just one heat capacity measurement of the hydroxide salt, the beams are observed to begin to flake and the platinum itself of the pan of the beams begins to discolor. In the most extreme circumstances, the beam's pan began to pull away from it, or chunks of it fell off entirely. This salt is clearly highly corrosive to equipment used to measure its properties. Caution and consideration of the salts toll on equipment and the costs associated should be used in the future before starting further experiments with this salt.

In addition to the corrosion, salt was also observed to creep out of the glassy carbon crucibles, sometimes causing the crucible to stick to the pan of the beam. Cleaning the beam when this happened proved difficult and was not always entirely successful.

5.2 Hydroxide Salt Volatility

The observed creeping of the hydroxide salts was cause for confusion, as the salts did not display such behavior with the glassy carbon that was used for the density measurements. However, consistently after each heat capacity measurement, the hydroxide salts were found to have left the crucible. Though, it is unclear if this was caused by creeping or by the salt boiling over or exploding. This caused the crucible to become stuck to the pan of the beam and caused the salt to come into contact with the alumina beams, thus speeding up the corrosion process.

One theory behind this behavior is that past a certain temperature, the NaOH-KOH salt will begin to dissociate into its base components [47]. At this point, the material becomes more volatile and less predictable. However, this phenomenon was not investigated during the experimentation of this paper. As such, there can be no definitive explanation. It is highly encouraged that a later work covers this, especially considering that the sponsors desired the salts properties be known for a wide range of temperatures up to 600C. Investigating this further may also aid in the preservation of the DSC beams which are notoriously expensive.

5.3 Peak Decomposition

In a prior section, it was noted that the BeF_2-NaF melting point could not successfully be determined because of the second peak of the heat flow curve being conjoined with the first. Here I intend to explain one solution to that problem which could not be executed out of a lack of time.

The solution is the process of decomposition of the two curves, a complex and unreliable technique with multiple methods. One method of decomposition was employed in [48] where they used a narrow peak method and principal component analysis. In this approach, they used a nonlinear iterative partial least squares algorithm to show that their spectra could be described by three linear principal component combinations and a residual matrix. Further analysis is done with the following equation in mind,

$$I(\lambda) = \sum_i \alpha_i I_i(\lambda)$$

Where I(λ) is the ith principal component spectrum, α_i is its weight, $\lambda$is the emission wavelength..

In [48], this complex technique is compared to the MCR-ALS algorithm which has the same goal. MCR-ALS, however, can be described as inferior due to it being iterative and based upon the initial estimate of the spectra in question.

The principal component analysis method and the MCR-ALS algorithm are just two examples of a plethora of algorithms that can be used to decompose a conjoined peak into two separate ones. However, the process of decomposition in general has a marked flaw. That being, many assumptions must be made to come to the conclusions that the algorithms come to. For this reason, these algorithms can, at best, be described as an estimate of the true value derived from the curves in question.

Due to the complexity of this process, it had not been done in time for this report. As such, the decomposition of that data is left to a future report.

Chapter 6

Conclusion

Three salts were examined in this study, FLiNaK, NaOH-KOH, and BeF_2-NaF. The latter two of these salts has the potential to be used within future molten salt reactor projects. For their use in a future reactor to be investigated, their thermal properties must be evaluated at a wide range of temperatures to account for the operating temperatures and the cases of operation failure. Though other studies have performed similar measurements, this study sought to perform the measurements at greater temperature ranges, with methods that provide great accuracy.

A few of the properties of interest are the melting point, the heat capacity, the vapor pressure, and the density. It is optimal for the melting point to be low so that the reactor can be operated at lower temperatures. Lower temperatures means that the system is safer overall. For this reason, melting temperature is one of the most important, if not the most important property to consider [1]. The heat capacity should be high since that would mean that the material is able to absorb heat without changing temperature too drastically. It is, in general, better to have a material that has more stable and predictable properties. The density is relevant to the heat transport and dimensions of a reactor. And finally, it is desirable for the vapor pressure to be low. If the vapor pressure is low, then that would imply greater stability at the higher temperatures of operation. After all, one of the worst things for a reactor is in increased amount of gas and pressure at the already high temperatures.

FLiNaK was used in this study as a way to test our systems before measuring the properties of the other salts. FLiNaK is reliable and well-studied considering it was one of the very first salts that were examined back in the 1900s when molten salts were first being researched. With FLiNaK, a calibration system was created for our density measurement setup. And FLiNaK was used to assess the reliability of our DSC/TGA setup. The results were excellent with the measured melting point coming within 0.5% of the expected melting point of FLiNaK.

Hydroxide salts, such as NaOH-KOH, have been under consideration for some time for their aptitude for storing energy. Of course, this characteristic makes them great coolant salts, but it also makes them great for a variety of purposes related to energy storage and transfer. In this study, the density and heat capacity of NaOH-KOH were measured. Density-temperature equations were determined and displayed that, within our range of 350-600C, the densities ranged from 1.48-1.66 g/cm^3 and, as expected, decreased with temperature. The densities also did not display a reliance on the composition of the salt. The heat capacity of our select hydroxide salt compositions did not show a trend based on the composition of salt either. They ranged from ~0.7 J/gC at higher temperatures to ~1.7 J/gC at lower temperatures across our range of 300-600C. In addition to our measurements, it was noticed that the hydroxide salts were both extremely prone to absorbing water, were very corrosive to our materials, and were volatile at higher temperatures. This makes the salt less useful in the context of a reactor. It is advised to conduct further experiments entirely under an inert gas and with caution to the higher temperature measurements. Furthermore, the salt should be examined at those higher temperatures to evaluated what exactly is going on with the volatility exhibited. The decrease of Cp with temperature can

be explained because both NaOH and KOH may decompose at high temperatures to form Na_2O and K_2O which have lower Cp. The decomposition may also influence accuracy of the measurements.

BeF_2-NaF is another candidate for the coolant of molten salt reactors. Its melting point is quite low compared to the other two salts of this study at a measured ~360C. Already this makes the salt a desirable candidate for coolant. Although the vapor pressure is not as low as the notoriously low vapor pressure of FLiNaK, it is not that much higher. Additionally, the heat capacity, though notably measured as higher in past studies, is somewhat agreeable. It is not as high as waters heat capacity of 4.8 J/gC [28], but it is not so low as to be concerning sitting at around 1.35 J/gC depending on the temperature. Still, that lower than expected heat capacity is notable. Overall, it seems that BeF_2-NaF, depending on the geometry of the reactor, has desirable properties.

On the other hand, BeF_2-NaF is an extremely toxic material that poses a danger and a risk to both researchers and future reactor operators. Even if the properties of the salt are desirable, if the salt poses such danger, then why use it? Surely, since MSR's are already high temperature reactors, the low melting point is not that important. One must weigh which properties of a salt truly matter, especially with a material that could hurt people.

So then, why is BeF_2-NaF still worthy of being considered and even an excellent option for a reactor coolant? This is due to the way that beryllium interacts within an MSR beyond just the properties that have been investigated in this report [49]. For an MSR, the presence of beryllium in the core allows the reactor to have an alpha-induced neutron source, an inherent neutron source. Photoneutrons build up as the reactor is operated, and so when the reactor is shut down the inherent neutron source can act as an installed source until the operation is restarted. The other reason is that addition of BeF_2 can reduce the melting temperature of the salt mixture. For this reason, beryllium, as toxic as it is, plays a crucial role in MSRs. Still, the toxicity must be acknowledged and extensive safeguards put into place in both the research and reactor settings.

In conclusion, two of the lesser understood salt candidates now have been further investigated. FLiNaK maintains its status as an excellent calibration standard. NaOH-KOH displays some desirable properties, but also displays an irksome volatility and an added difficulty in researching it due to its hydrophilic nature. BeF_2-NaF has excellent properties with a beautifully low melting point, but it still must be recognized for the danger that it could pose.

Bibliography

[1] D. F. Williams. *Assessment of Candidate Molten Salt Coolants for the NGNP/NHI Heat-Transfer Loop*. Oak Ridge National Laboratory, 2006.

[2] D. F. Williams, L. M. Toth, and K. T. Clarno. *Assessment of Candidate Molten Salt Coolants for the Advanced High-Temperature Reactor (AHTR)*. Oak Ridge National Laboratory, 2006.

[3] J. Park, W. Zhuo, C. Ridder, A. Leaong, and J. Zhang. *Thermophysical and thermodynamic properties of NaF-BeF2-UF4-ZrF4 fuel salt.* Materials Today Communications, 2023.

[4] W. D. Powers, S. I. Cohen & N. D. Greene (1963) *Physical Properties of*

Molten Reactor Fuels and Coolants, Nuclear Science and Engineering, 17:2, 200-211, DOI:

10.13182/NSE63-5

[5] D.J. Rogers, T. Yoko, and G.J. Janz. *Fusion Properties and Heat Capacities of the Eutectic LiF-NaK-KF Melt*. J. Chem, vol.27, p366-367, 1982.

[6] J. Schorne-Pinto, et al. *Thermal Property Modeling and Assessment of the physical Properties of FLiNaK.* ACS Applied Energy Materials, vol 7, p4016-4029, 2024.

[7] I. Langmuir. *The Vapor Pressure of Metallic Tungsten*. Second Series, Vol. 11 No. 5, 1913.

[8] S. Giani, R. Riesen, and J.E.K. Schawe. *An Indirect Method for Vapor Pressure and Phase Change Enthalpy Determination by Thermogravimetry*. Springer Nature, 2018.

[9] M. Yamawaki, M. Hirai, M. Yasumoto, and M. Kanno. *Mass Spectrometric Study of Vaporization of Lithium Fluoride*. Journal of Nuclear Science and Technology, vol. 19, pp. 563-570, 1982.

[10] D.L. Hildenbrand, W.D. Hall, F. Ju, and N.D. Potter. *Vapor Pressures and Vapor Thermodynamic Properties of Some Lithium and Magnesium Halides*. Journal of Chemical Physics, vol. 40, 2882, 1964.

[11] R.S. Scheffee and J.L. Margrave. *Vapor Pressure Equations for Species over Solid and Liquid LiF*. Journal of Chemical Physics, vol. 31, 1682, 1959.

[12] M. Eisenstadt, G.M. Rothberg, and P. Kusch. *Molecular Composition of Alkali Fluoride Vapors*. Journal of Cheical Physics, vol. 29, 797, 1958.

[13] J. McMurray, A. McAlister, J. McFarlane, and J. Kurley. *Thermal Analysis of Non-actinide Bearing Salt.* ORNL, 1616, 2020.

[14] Y.S. Choi, H. Park, and T. Lho. *Evaporation Properties of FLiNaK with Plasma Interaction.* Fusion Science and Technology, 2017.

[15] W.R. Grimes, D.R. Cuneo, F.F. Blankenship, G.W. Keilholtz, H.F. Poppenkiek, M.T. Robinson,

Chemical Aspects of Molten-Fluoride-Salt Reactor Fuels, in: J.A. Lane, H.G. MacPherson, F. Maslan

(Eds.), Fluid Fuel React., Addison-Wesley Publishing Company, Inc., Reading, Massachusetts, 1958:

pp. 569–594.

[16] R. C. Gallagher, et al. *Assessment of molten eutectic LiF-NaK-KF density through experimental determination and semi-empirical modeling*. ORNL.

[17] A.M. Long, et al. *Remote Density Measurements of Molten Salts via Neutron Radiography*. Journal of Imaging, 7, 88. 2021.

[18] M. Salanne, et al. *Heat-transport properties of molten fluorides: Determination from first-principles*. Journal of Fluorine Chemistry, 130, 38-44. 2009.

[19] J. Cibulková, M. Chrenková, R. Vasiljev, V. Kremenetsky, M. Boča, Density and viscosity of the

(LiF + NaF + KF)eut (1) + K 2TaF7 (2) + Ta2O5 (3) melts, J. Chem. Eng. Data. 51 (2006) 984–987.

[20] H.W. Otto and R.P. Seward. *Phase Equilibria in the Potassium Hydroxide-Sodium Hydroxide*

System. Journal of Chemical and Engineering Data, 9-4, 1964.

[21] S. Dai et al. *Highly-efficient molten NaOH-KOH for organochlorine destruction: Performance and mechanism*. Environmental Research.

[22] D.D. Jackson and J.J. Morgan. *Measurement of Vapor Pressures of Certain Potassium Compounds.* The Journal of Industrial and Engineering Chemistry, 13-2, 1920.

[23] E.B. Hoyt. *Vapor Pressure of Strong Sodium Hydroxide Solutions*. Allied Chemical Corp., 1967.

[24] G.J. Janz and R.P.T. Tomkins. *Physical Properties Data Compilations Relevant to Energy Storage*. Molten Salts Data Center, 1981.

[25] Y. Takahashi, M. Kamimoto, et al, *Investigation of Latent Heat-Thermal Energy Storage Materials. IV. Thermoanalytical Evaluation of Binary Eutectic Mixtures of NaOH With LiOH or KOH.*, Thermochimica Acta, 1987.

[26] Y. M. Baikov and V.M. Egorov. *Solid-Hydroxide Protonic Conductors: Superionic Conductivity, Phase Transitions, Isotiopic Effect, and Self-Organizaed Microheterogeneity.* Ioffe Physiotechnical Institute, 2009.

[27] L.C. Thomas, Why Modulated DSC?: An Overview and Summary of Advantages and Disadvantages Relative to Traditional DSC, (2005).

[28] Chase, M.W., Jr., *NIST-JANAF Themochemical Tables, Fourth Edition*, J. Phys. Chem. Ref. Data, Monograph 9, 1998, 1-1951.

[29] B.V. Patrov and V.P. Yurkinskii. *Surface tension and density of a sodium hydorxide melt*. Russion Journal of Applied Chemistry, 77, 2029-2030. 2004.

[30] X. LI, R. Cui, Y. Song, and Y. Gong. *Insights on the microstructural correlations of density and specific heat capacity for halophilic fission products and NaF-BeF2 molten mixtures.* Journal of Nuclear Materials, 599, 2024.

[31] K.A. Sense, R.W. Stone, Vapor Pressures and Molecular Composition of Vapors of the Sodium Fluoride-Beryllium Fluoride system, J. Phys. Chem. 62 (1958).

[32] S.I. Cohen, W.D. Powers, N.D. Greene, *A Physical Property Summary For ANP Fluoride Mixtures*, Oak Ridge, Tennessee, 1956.

[33] A. Redkin, A. Khudorozhkova, E. Il'ina, S. Pershina, P. Mushnikov, A. Isakov, Y. Zaikov,

A. Kataev, M. Laptev, Density and heat capacity of some molten mixtures in system LiF-BeF_2-

UF_4, J. Mol. Liq. 341 (2021) 1–7. https://doi.org/10.1016/j.molliq.2021.117215.

[34] B. D'Aguanno, M. Karthik, A.N. Grace, A. Floris, Thermostatic properties of nitrate molten salts and their solar and eutectic mixtures, Sci. Rep. 8 (2018) 1–15.

[35] A.S. Teja, Simple Method for the Calculation of Heat Capacities of Liquid Mixtures, J. Chem. Eng. Data. 28 (1983) 83–85.

[36] M. Liu, et al. *Mapping relationships between cation-F bonds and the heat capacity, thermal conductivity, viscosity of molten NaF-BeF2*. Journal of Molecular Liquids, 354, 2022.

[37] G.J. Janz. *Thermodynamic and Transport Properties for Molten Salts: Correlation Equations for Critically Evaluated Density, Surface Tension, Electrical Conductance, and Viscosity Data*. Journal of Physical and Chemical Reference Data, 17. 1988.

[38] V. Afonichkin, A. Bovet, and V. Shishkin. *Salts purification and voltammetric study of the electroreduction of U(IV) to U(III) in molten LiF-ThF4*. Journal of Nuclear Materials, 419, 2011.

[39] P. Soucek, et al. *Syntehsis of UF4 and ThF4 by HF gas fluorination and re-determination of the UF4 melting point*. Journal of Fluorine Chemistry, 200, 2017.

[40] J.H. Shaffer, Preparation of MSRE Fuel, Coolant, and Flush Salts, in: R.B. Briggs (Ed.), Molten-Salt React. Progr. Semiannu. Prog. Rep. Period End. July 31, 1964, 35th ed., Oak Ridge National Laboratory, Oak Ridge, Tennessee, 1964: pp. 288–303.

[41] M. Eisenstadt, G.M. Rothberg, P. Kusch, Molecular composition of alkali fluoride vapors, J. Chem. Phys. 29 (1958) 797–804. https://doi.org/10.1063/1.1744593.

[42] J. Park, A. Leong, J. Zhang, Density Measurements of Molten Salts, J. Chem. Eng. Data. 68 (2023) 1892–1898.

[43] G.J. Janz, F.W. Dampier, G.R. Lakshminarayanan, P.K. Lorenz, R.P.T. Tomkins, *Molten Salts: Volume 1, Electrical Conductance, Density, and Viscosity Data*, Washington, D.C., 1968.

[44] Archer, Donald G., *Thermodynamic properties of Synthetic Sapphire, Standard Reference Material 720 and the effect of temperature-scale differences on thermodynamic properties*, Journal of Physical and Chemical Reference Data, 1993. 22, 1441.

[45] O. Benes and R.J.M. Konings. *Thermodynamic properties and phase diagrams of fluoride salts for Nuclear Applications.* Journal of Fluorine Chemistry, 130, 22-29, 2009.

[46] W. J. Boettinger, U. R. Kattner, K. W. Moon, and J. H. Perepezko. *DTA and Heat-flux DSC*

Measurements of Alloy Melting and Freezing. NIST, 960-15, 2006.

[47] R.F. Porter and R.C. Schoonmaker. *Gaseous Species in the NaOH-KOH System*. Cornell University Department of Chemistry, 1958.

[48] E. Tsibulskaya and N. Maslov. *Decomposition of multi-component fluorescence spectra by narrow peak method based on principle component analysis*. Journal of Chemometrics, 2021.

[49] R.M. Ji, et al. *Study on inherent neutron sources in MSR.* Shanghai Institute of Applied Physics, 2018.